THE JOURNAL OF PHYSICAL CHEMISTRY A

 VOLUME 107, NUMBER 35, SEPTEMBER 4, 2003

FEATURE ARTICLE

Geometric Phase Effects in Chemical Reaction Dynamics and Molecular Spectra

Brian K. Kendrick

Theoretical Division (T-12, MS-B268), Los Alamos National Laboratory, Los Alamos, New Mexico 87545

Received: August 12, 2002; In Final Form: June 18, 2003

The theoretical methodology for including the effects of the geometric phase in quantum reactive scattering and bound-state calculations is reviewed. Two approaches are discussed: one approach is based on solving the standard Born−Oppenheimer equation but with double-valued boundary conditions, and the second approach is based on solving a generalized Born−Oppenheimer equation with single-valued boundary conditions. The generalized Born−Oppenheimer equation contains a vector potential which is mathematically equivalent to that of a magnetic solenoid. The recently developed numerical methodology for solving the generalized Born−Oppenheimer equation is reviewed, and several applications of this methodology in chemical reaction dynamics and molecular spectra are discussed. New results from accurate six dimensional quantum reactive scattering calculations for the $D + H_2(v, j) \rightarrow HD(v', j') + H$ and $H + H_2(v, j) \rightarrow H_2(v', j') + H$ reactions are presented. These calculations are performed both with and without the geometric phase. The geometric phase calculations are done using both the double-valued basis set approach and vector potential approach. The effects of the geometric phase in the reaction probabilities, integral, and differential cross sections are investigated as a function of scattering energy and total angular momentum J.

I. Introduction

The standard theoretical treatment of chemical reaction dynamics and molecular vibrations is based on the separation of the total molecular motion into fast and slow parts. The fast motion corresponds to the motion of the electrons, and the slow motion corresponds to the motion of the nuclei. The theoretical foundation for the separation of the electronic and nuclear motion was first developed by Born and Oppenheimer.[1] In this approach, the total molecular wave function is expanded in terms of a set of electronic eigenfunctions which depend parametrically on the nuclear coordinates. The expansion coefficients are the nuclear motion wave functions which satisfy a matrix Schrödinger equation which includes off-diagonal coupling matrix elements with respect to the electronic quantum numbers. The smallness of the electronic mass (m_e) relative to the nuclear mass (m_N) is used to obtain an asymptotic expansion of the total molecular wave function, energy, and other quantities of interest in terms of the small parameter $\kappa = (m_e/m_N)^{1/4}$.[2−4] To lowest order in κ, the off-diagonal coupling terms can often be ignored for low-energy collisions, small amplitude molecular vibrations, and nondegenerate electronic states. In this case, the total molecular wave function can be expressed in terms of a single electronic state (usually the ground state). Thus, to a good approximation, the nuclear motion is governed by an effective Schödinger equation whose potential energy surface is determined by solving the Schödinger equation for the ground electronic state at each nuclear geometry. This one-state approximation is often referred to as the "Born−Oppenheimer approximation" and has been the foundation for the modern theory of electronically adiabatic processes. For high-energy collisions or degenerate electronic states, the Born−Oppenheimer approximation can break down, and more than one electronic state must often be included. For example, high-energy collisions give rise to electronically nonadiabatic processes (i.e., collision processes which change the electronic quantum numbers).[5] Another situation for which the standard Born−Oppenheimer method becomes inadequate is when a conical intersection occurs between the ground and an excited electronic state. Conical intersections can alter the nuclear dynamics even for low-energy collisions or vibrational motion

10.1021/jp021865x CCC: $25.00
Published on Web 08/12/2003

for which the one-state approximation is valid. In this article, we consider the modifications to the standard Born−Oppenheimer method which are required in order to account for the effects of conical intersections on the nuclear dynamics for low-energy collisions and vibrational motion on a ground-state electronic potential energy surface.

In 1963, Herzberg and Longuet-Higgins[6] showed that a real adiabatic electronic wave function changes sign (i.e., it is a double-valued function) when the nuclear coordinates traverse a closed path which encircles a conical intersection. In order for the total molecular wave function to remain single-valued, a compensating sign change must also occur in the nuclear motion wave function. Furthermore, for molecules with two or more identical nuclei, the sign change must be accounted for in order for the total molecular wave function to satisfy the correct Bose−Fermi statistics under an interchange of any two identical nuclei. In 1979, Mead and Truhlar[7,8] discussed two approaches for including the sign change in the nuclear motion wave function. In one approach, a real double-valued electronic wave function is used and the correct nuclear motion wave functions are obtained by solving the standard Schödinger equation for the nuclear motion but with double-valued boundary conditions. In the second approach, a *complex* single-valued electronic wave function is used, and the correct nuclear motion wave functions are obtained by solving a generalized Schödinger equation for the nuclear motion with single-valued boundary conditions. The complex single-valued electronic wave function is obtained by multiplying the real double-valued electronic wave function by a complex phase factor which is a function of the nuclear coordinates. This phase factor changes sign for any closed path which encircles a conical intersection so that the complex electronic wave function is single-valued. The electronic Schödinger equation is unchanged by the phase transformation so that the complex single-valued electronic wave function satisfies the same eigenvalue equation as the real double-valued electronic wave function. However, the Schödinger equation for the nuclear motion acquires a vector potential (i.e., the momentum operator $\mathbf{p} \rightarrow \mathbf{p} - \mathbf{A}$). This vector potential comes from the gradient operator with respect to the nuclear coordinates acting on the complex phase factor. The vector potential is nontrivial (i.e., it cannot be transformed or gauged away by using a single-valued phase transformation) and is mathematically equivalent to that of a "magnetic solenoid" centered at the conical intersection. The resulting Schödinger equation for the nuclear motion is identical to that of a charged particle moving in the presence of a magnetic solenoid. If the nuclear motion wave function has significant amplitude along the entire minimum energy pathway encircling a conical intersection, significant interference effects will occur which can significantly alter the nuclear dynamics. These effects can occur for relatively small collision and vibrational energies which are much smaller than the energy of the conical intersection. The collision or vibrational energy only needs to be larger than all of the potential energy barriers which may occur along the minimum energy pathway encircling the conical intersection. Mead later called this effect the "molecular Aharonov−Bohm effect".[9] In 1984, Berry[10] considered a general quantum system with parametric time dependence undergoing a cyclic adiabatic time evolution. He showed that the sign change which occurs in the "molecular Aharonov−Bohm effect" is a special case of the more general geometric phase often referred to as "Berry's phase". Berry's influential paper generated much theoretical and experimental interest in this effect which continues to this day.

Section 2 presents the generalized Born−Oppenheimer equation for the nuclear motion which takes into account the geometric phase effects due to a conical intersection. Section 3 reviews the recently developed numerical methods for solving the generalized Born−Oppenheimer equation. Several applications using this methodology are also discussed. Section 4 presents new results from accurate full dimensional quantum reactive scattering calculations for two fundamental chemical reactions: $H + H_2 \rightarrow H_2 + H$ and $D + H_2 \rightarrow HD + H$. A conical intersection occurs in the H_3 molecule when all three of the internuclear distances are equal (i.e., D_{3h} geometries). The effects of the geometric phase are investigated by solving both the standard and generalized Born−Oppenheimer equations for the nuclear motion and comparing the results. The reaction probabilities, integral, and differential cross sections for each of these reactions are presented as a function of total energy and total angular momentum (J). Section 5 presents some conclusions regarding the importance of geometric phase effects in chemical reaction dynamics and molecular vibrational spectra.

II. Generalized Born−Oppenheimer Method

The molecular Schödinger equation is given by

$$H \Psi_{\text{tot}} = E \Psi_{\text{tot}} \tag{1}$$

where Ψ_{tot} is the total molecular wave function, H is the total molecular Hamiltonian, and E is the total energy. We restrict our present treatment to triatomic molecules so that there are six nuclear coordinates relative to the center of mass. Three of these six are internal coordinates which are functions of the three internuclear distances. The remaining three are angular coordinates which specify the orientation of the body-frame relative to the space-frame and are usually taken to be the three Euler angles. The six nuclear coordinates are denoted as $\mathbf{x} = (x, \hat{x})$ where x and $\hat{x}$ denote the three internal and three angular coordinates, respectively.

After separating out the center of mass motion, we can express H in space-frame coordinates as

$$H \equiv -\frac{\hbar^2}{2\mu} \nabla^2 + h(x) \tag{2}$$

where ∇^2 is the six-dimensional Laplacian with respect to the six nuclear coordinates $\mathbf{x}$, μ is the three body reduced mass $\mu \equiv (m_A\, m_B\, m_C/(m_A + m_B + m_C))^{1/2}$, and $h(x)$ is the electronic Hamiltonian which depends parametrically on the three internal nuclear coordinates.

We neglect all electronic angular momentum (spin and orbital) so that the space-frame electronic eigenfunctions (φ_n) depend parametrically on the three internal nuclear coordinates x and can be chosen real orthogonal with real eigenvalues (V_n)[11]

$$h(x)\, \varphi_n(\mathbf{r}; x) = V_n(x)\, \varphi_n(\mathbf{r}; x) \tag{3}$$

where $\mathbf{r}$ denotes all of the electronic coordinates. From now on, we assume that accurate solutions to eq 3 are available or can be readily calculated.

The total molecular wave function can be expanded in terms of the electronic eigenfunctions

$$\Psi_{\text{tot}} = \sum_{n=0}^{N} \Psi_n(\mathbf{x})\, \varphi_n(\mathbf{r}; x)\, \psi^{\text{ns}} \tag{4}$$

where the expansion coefficients $\Psi_n(\mathbf{x})$ are the nuclear motion wave functions, and ψ^{ns} is the nuclear spin wave function. The

number of electronic states N is in general infinite. Fortunately, the smallness of the Born−Oppenheimer parameter κ allows one to truncate this infinite sum to some finite number N. If one substitutes eq 4 into eq 1, multiplies on the left by $\varphi_n(\mathbf{r}; \mathrm{x})$, integrates over $\mathbf{r}$, and uses eq 3, one obtains the following matrix equation for the nuclear motion wave function to lowest order in κ ($n = 0, 1, 2, ..., N$)[12−14]

$$\sum_{m=0}^{N}\left[\frac{\hbar^2}{2\mu}\sum_{k=0}^{N}(-i\,\delta_{nk}\nabla - \mathbf{A}_{nk}(\mathrm{x}))\cdot(-i\,\delta_{km}\nabla - \mathbf{A}_{km}(\mathrm{x})) + \epsilon_{nm}(\mathrm{x})\right]\Psi_m(\mathbf{x}) = E\,\Psi_n(\mathbf{x}) \quad (5)$$

where the vector nonadiabatic coupling matrix elements are given by

$$\mathbf{A}_{nm}(\mathrm{x}) = i\,\langle\varphi_n(x)|(\nabla|\varphi_m(\mathrm{x})\rangle) \quad (6)$$

The effective scalar potential is given by[12−14]

$$\epsilon_{nm}(\mathrm{x}) = V_n(\mathrm{x})\,\delta_{nm} - \frac{\hbar^2}{2\mu}\sum_{l\neq n,m}\langle\varphi_n(\mathrm{x})|(\nabla|\varphi_l(\mathrm{x})\rangle)\cdot\langle\varphi_l(\mathrm{x})|(\nabla|\varphi_m(\mathrm{x})\rangle) \quad (7)$$

The scalar potential given in eq 7 contains mass dependent contributions which involve derivative coupling matrix elements between the electronic subspace of interest and the excited electronic states. For low collision energies or small amplitude vibrational motion, these contributions have the effect of a small correction (proportional to κ^4) to the potential energy $V_n(\mathrm{x})$. From now on, we ignore these small corrections and take $\epsilon_{nm}(\mathrm{x}) = V_n(\mathrm{x})\,\delta_{nm}$. However, near a conical intersection (i.e., for high collision energies which approach the energy of the conical intersection), these contributions are not necessarily small. For diatomic molecules, they have been evaluated using specialized,[15,16] and more conventional,[17] electronic structure techniques and also have been measured experimentally.[18]

In many applications, we can truncate the sum in eq 4 to only one term. This case is often referred to as the "Born−Oppenheimer approximation", and the molecular wave function is given by

$$\Psi_{\mathrm{tot}} \approx \Psi_0(\mathbf{x})\,\varphi_0(\mathbf{r}; x)\,\psi^{\mathcal{N}} \quad (8)$$

where $n = 0$ denotes the ground electronic state. For high collision energies or degenerate electronic states, more terms in the sum over n must often be included. From now on, we assume that eq 8 is valid and drop the subscript on the nuclear and electronic wave functions with the understanding that they denote the ground electronic state. The Born−Oppenheimer eq 5 for the nuclear motion becomes

$$\left[-\frac{\hbar^2}{2\mu}\nabla^2 + V(\mathrm{x})\right]\Psi(\mathbf{x}) = E\,\Psi(\mathbf{x}) \quad (9)$$

In the derivation of eq 9, we used the fact that $\langle\varphi(\mathrm{x})|\nabla|\varphi(\mathrm{x})\rangle = 0$ which is straightforward to prove by differentiating the normalization equation $\langle\varphi(\mathrm{x})|\varphi(\mathrm{x})\rangle = 1$ and using the fact that $|\varphi(\mathrm{x})\rangle$ is real.

We denote the d-dimensional internal nuclear parameter space by $\mathscr{M}$ ($d = 3$ for triatomics) and the subspace of $\mathscr{M}$ for which a conical intersection occurs by $\mathscr{D} \subset \mathscr{M}$. The subspace $\mathscr{D}$ is of dimension $d - 2$, and for triatomic molecules it is a one-dimensional curve in the three-dimensional nuclear parameter space $\mathscr{M}$.[6,19] Two conditions $u(x) = 0$ and $v(x) = 0$ define the subspace $\mathscr{D}$, and these can be expressed in terms of any two diagonal cofactors of the matrix $\mathbf{w}(x) \equiv \mathbf{h}(x) - \mathbf{I}\,V_0(x)$ where $\mathbf{h}$ is the electronic Hamiltonian and V_0 is the ground-state eigenvalue.[20] In an infinitesimal region near $\mathscr{D}$, the relevant part of the electronic Hamiltonian is a 2×2 matrix of the form[7,19]

$$h(\mathrm{x}) = -\begin{pmatrix}\delta u & \delta v\\ \delta v & -\delta u\end{pmatrix} = -r\begin{pmatrix}\cos\eta & \sin\eta\\ \sin\eta & -\cos\eta\end{pmatrix} \quad (10)$$

where $\delta u(x)$ and $\delta v(x)$ are infinitesimal displacements from the origin in the two-dimensional Cartesian space spanned by $u\,\mathbf{e}_u$ and $v\,\mathbf{e}_v$ (see Figure 1). The polar coordinates are denoted by (r, η) where r is the radial distance from the origin in uv space and η is the azimuthal angle around the origin. The two eigenvalues of eq 3 are $V_{\pm}(x) = \pm r$ which correspond to the upper and lower cones in Figure 1. The two corresponding eigenvectors are given by

$$\varphi^{+} = \begin{pmatrix}-\sin\frac{\eta}{2}\\ \cos\frac{\eta}{2}\end{pmatrix},\ \varphi^{-} = \begin{bmatrix}\cos\frac{\eta}{2}\\ \sin\frac{\eta}{2}\end{bmatrix} \quad (11)$$

It is clear that, because of the half-angle functional dependence upon the azimuthal angle η, these eigenvectors change sign (i.e., are double-valued) for any closed path in the nuclear parameter space for which η changes by 2π. Equation 11 is valid only in the infinitesimal region near the conical intersection. However, the sign change (double-valuedness) exists *globally*. That is, any closed path in $\mathscr{M}$ which encircles $\mathscr{D}$ (no matter how far away from $\mathscr{D}$) results in a sign change in the adiabatic ground-state real electronic eigenvector.[21] The *global* expression for the angle η is given by $\eta(x) \equiv \tan^{-1}(v(x)/u(x))$ which is in general a complicated function of the three internal nuclear coordinates.[22] Recently, techniques have been developed to compute $\eta(x)$ for a general polyatomic molecule.[20,23−25] However, for triatomic molecules (such as H_3, HO_2, and Na_3), a suitable functional form for $\eta(x)$ can often be derived analytically.[7,11] It is important to realize that the functional forms of $u(x)$ and $v(x)$ are not unique. Hence, $\eta(x)$ is not unique. The

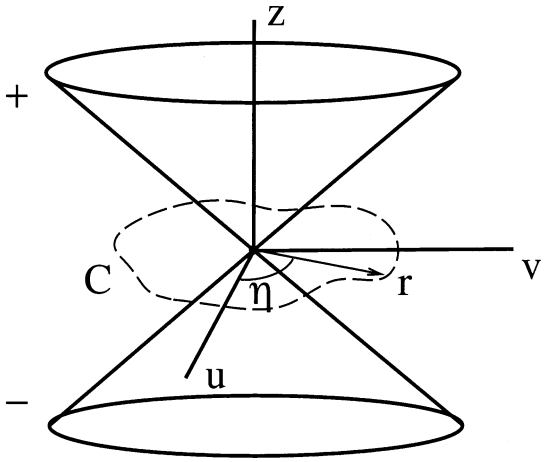

Figure 1. Perspective plot of a two-dimensional slice of a potential energy surface near a conical intersection. The degeneracy point is located at the origin in the uv plane. The radial distance from the intersection is denoted by r and the azimuthal angle around the intersection denoted by η. The adiabatic ground-state real electronic wave function changes sign for any closed path in uv space which encircles the origin (such as the dashed curve C).

only requirement is that $\eta(x)$ change by 2π for *any* closed path in $\mathcal{M}$ which encircles $\mathcal{D}$. This freedom in choosing η is called "gauge freedom" and different choices for η are related by $U(1)$ gauge transformations.[7,11,19,20,26]

Following Mead and Truhlar,[7] we multiply the real adiabatic electronic wave function by a complex phase

$$\varphi^{\mathcal{C}}(\mathbf{r}; x) \equiv \exp\left(i\frac{l}{2}\eta(x)\right) \varphi(\mathbf{r}; x) \tag{12}$$

where l is an *odd integer* and $\eta(x)$ is the azimuthal angle discussed above which changes by 2π for any nuclear motion which encircles a conical intersection. The complex phase factor cancels the sign change from the real electronic wave function $\varphi(\mathbf{r}; x)$ giving rise to a complex *single-valued* electronic wave function $\varphi^{\mathcal{C}}(\mathbf{r}; x)$. It is straightforward to show that the different choices for l are related by gauge transformations.[7] Hence, the choice of l is a matter of convenience although larger values of l cause the numerical calculations to converge more slowly.[11,26]

Using eq 12 and repeating the same steps which lead to eq 9, we obtain the generalized Born−Oppenheimer equation for the nuclear motion[7,11−14,19]

$$\left[\frac{\hbar^2}{2\mu}(-i\nabla - \mathbf{A}(x))^2 + V(x)\right] \Psi^{\mathcal{C}}(\mathbf{x}) = E\,\Psi^{\mathcal{C}}(\mathbf{x}) \tag{13}$$

where the nuclear motion wave function $\Psi^{\mathcal{C}}(\mathbf{x})$ is *single-valued* and $\mathbf{A}(x)$ is the vector potential defined as

$$\mathbf{A}(x) \equiv i\langle\varphi^{\mathcal{C}}(x)|(\nabla|\varphi^{\mathcal{C}}(x)\rangle) \tag{14}$$

Substituting eq 12 into eq 14, we can write the vector potential as

$$\mathbf{A}(x) = -\frac{l}{2}\nabla\,\eta(x) \tag{15}$$

Equation 15 has the same mathematical form as the vector potential of a magnetic solenoid located at the conical intersection.[7−9,19] By taking the curl of eq 15, we find that the corresponding "magnetic field" is zero everywhere except at the conical intersection where it has a delta function singularity

$$\mathbf{B}(x) \equiv \nabla \times \mathbf{A}(x) = -l\,\pi\,\delta(x)\,\mathbf{e}_z \tag{16}$$

where $\mathbf{e}_z$ points along the z axis perpendicular to the $u\upsilon$ plane with the conical intersection located at the origin (see Figure 1).[7−9,19] Equation 16 has the same mathematical form as the magnetic field of an infinitely thin and infinitely long magnetic solenoid centered at the conical intersection. Of course, the vector potential of eq 15 and its associated magnetic field given by eq 16 do not represent a real magnetic field. They come from the diagonal derivative coupling term which couples the nuclear and electronic motion (see eq 14).

The geometric phase (β_g) can be expressed as the line integral of $\mathbf{A}$ along a closed path $\mathcal{C}$ in $\mathcal{M}$ which encircles the degeneracy subspace $\mathcal{D}$[7−10,19,25]

$$\beta_g = \oint_C \mathbf{A}\cdot d\mathbf{l} \tag{17}$$

By using Stokes's theorem, we can express the line integral of $\mathbf{A}$ as a surface integral of $\mathbf{B}$ which shows that the geometric phase (β_g) is equal to the "flux" of the "magnetic field" through the surface S enclosed by C

$$\beta_g = \int_S \mathbf{B}\cdot d\mathbf{s} \tag{18}$$

Upon substituting eq 15 into eq 17 or eq 16 into eq 18, we find that $\beta_g = -l\pi$ which corresponds to a phase factor of $\exp(-il\pi) = -1$. Thus, the sign change associated with a conical intersection can be given a geometrical interpretation. Equations 17 and 18 can be generalized to higher dimensions using the language of differential geometry. Equation 17 can be expressed as the line integral of a connection 1-form along the closed path $\mathcal{C}$ and the phase factor $\exp(i\beta_g)$ the associated holonomy. Similarly, eq 18 can be expressed as the surface integral of a curvature 2-form over the surface S enclosed by $\mathcal{C}$.[10,19,27−31]

III. Numerical Methodology for Solving the Generalized Born−Oppenheimer Equation

Although the generalized Born−Oppenheimer eq 13 was first derived in 1979, numerical techniques for solving this equation were developed only recently. Part of this delay is due to the singular nature of the vector potential which exhibits a r^{-1} singularity where r denotes the radial distance from the conical intersection. Thus, until recently, geometric phase effects were included in scattering and bound-state calculations by solving the standard Schödinger eq 9 but with double-valued boundary conditions. For example, the H_3 molecule contains a conical intersection which occurs for equilateral triangle (D_{3h}) geometries. If one uses symmetrized hyperspherical coordinates, then double-valued boundary conditions are relatively straightforward to implement for this molecule by choosing the angle η (see Figure 1) equal to the azimuthal angle ϕ of the 2D hypersphere. Thus, geometric phase effects can be included in the calculations by solving the standard Born−Oppenheimer eq 9 but expanding the solutions in terms of a double-valued basis set such as $\exp[i(m + 1/2)\,\phi]$ (where m is an integer). This is the approach used by Kuppermann and co-workers.[32,33] However, for other coordinate systems, for more complicated molecules, or when the conical intersection is not located at the symmetry point of the hyperspherical coordinates, the double-valued boundary conditions can be difficult to implement. For these more complicated cases, the vector potential approach which is based on solving the generalized Born−Oppenheimer eq 13 with single-valued boundary conditions is often more convenient. In 1994, Wu, Wyatt, and D'Mello[34] included geometric phase effects in scattering calculations for a model X_3 system using the vector potential approach. The motivation for using the vector potential approach in their calculations was that double-valued boundary conditions are difficult to implement in Jacobi coordinates. The development of numerical methods for using the vector potential approach to include geometric phase effects in scattering and bound-state calculations for a real molecule occurred in 1996.[11,26] This methodology uses symmetrized hyperspherical coordinates and is capable of treating multiple conical intersections located at arbitrary points on the 2D hypersphere. In the first applications using this method, the location of a conical intersection on the 2D hypersphere was taken to be independent of hyper-radial coordinate ρ.[11,26] In this case, the angle η is a function of the two hyperangles (θ, ϕ). The method was later generalized so that it could also treat the dependence of η on ρ.[35] The vector potential approach has been applied to low-energy inelastic scattering of $H + O_2(v, j) \rightarrow H + O_2(v', j')$,[11,26,35,36] to quantum reactive scattering of $H + D_2(v, j) \rightarrow HD(v', j') + D$[37] and $D + H_2(v, j) \rightarrow HD(v', j') + H$,[38] and to bound state calculations of HO_2 [35] and Na_3.[36,39] In this section, we review the numerical difficulties associated with the vector potential approach and discuss the effects of the geometric phase on the results of the scattering and bound state calculations mentioned above.

As mentioned above, our theoretical approach is based on symmetrized hyperspherical coordinates $x = (\rho, \theta, \phi)$.[40−43] The radial coordinate ρ corresponds to a symmetric stretch motion, the polar angle θ represents a bending type motion where $\theta = \pi/2$ corresponds to linear geometries and $\theta = 0$ corresponds to T-shaped arrangements (equilateral triangles for equal mass nuclei), and the azimuthal angle ϕ corresponds to an internal kinematic rotation (i.e., a pseudorotational motion). The body-frame z axis is chosen perpendicular to the plane of the triatomic molecule and the body-frame x and y axes are chosen to lie along the instantaneous principal axes of inertia (i.e., the Q and q vectors of ref 44, respectively). The orientation of the body-frame relative to the space-frame is given by the three Euler angles so that the collective set of six coordinates is given by $\mathbf{x} = (\rho, \theta, \phi, \alpha, \beta, \gamma)$. The Schödinger equation for the nuclear motion is solved in two steps.[44] In the first step, the radial variable ρ is partitioned into a large number of "sectors" and the five dimensional surface (angular) differential equation is solved with ρ fixed at the center of each sector. This step is independent of the scattering energy. The surface solutions are used to compute the potential coupling and overlap matrixes which appear in the coupled-channel (CC) radial equations. In the second step, the CC radial equations are solved at each scattering energy using a log-derivative propagation technique.[45,46] Once we have solved the CC radial equations, we apply the boundary conditions to the log-derivative matrix at large ρ to obtain the scattering matrix $\mathbf{S}$.[37,44] This scattering matrix contains all of the energetically open initial and final diatomic states.

The five dimensional surface function solutions are expanded in terms of a hybrid basis set consisting of a discrete variable representation (DVR)[47−49] in the hyperangle θ, a finite basis representation (FBR) in the azimuthal angle ϕ, and the appropriate set of normalized Wigner $\tilde{D}(\alpha, \beta, \gamma)$ functions.[50] The hybrid basis set accurately treats *both* of the Eckart[51] singularities which occur in the kinetic energy operator at the north pole and equator of the 2D hypersphere in (θ, ϕ) for all values of total angular momentum J (see ref 50 for details). This basis set also allows for an accurate treatment of geometric phase effects and is highly parallelizable.[37,52] The surface function Hamiltonian is diagonalized in parallel using a parallel implementation of the implicitly restarted lanzcos method (IRLM).[53−55]

A careful choice of the numerical quadrature scheme and a large set of quadrature points are required in order to obtain accurate matrix elements of the vector potential terms in eq 13.[11] The singularities in the terms involving $\mathbf{A}^2$ are the most troublesome because they involve r^{-2}. The volume element cancels one of the r^{-1} singularities but the integration of the remaining r^{-1} singularity gives rise to a divergent logarithmic function. Fortunately, the potential energy surface $V(x)$ is highly repulsive near a conical intersection so that, for low collision energies, the nuclear motion wave function has essentially zero amplitude near the conical intersection. Thus, the problem with the singular $\mathbf{A}^2$ terms can be handled by introducing a cutoff so that when $\mathbf{A}^2 > A_{\text{cut}}$, we set $\mathbf{A}^2 = A_{\text{cut}}$. The cutoff allows the numerical integrals to converge. The cutoff parameter A_{cut} is determined from convergence studies and is increased until the solutions become insensitive to it.[11,35,37] For high collision energies, more electronic states must be included and the vector potential approach must be generalized to include the off-diagonal matrix elements which couple the different electronic states (see eq 5). For more details on nonadiabatic methods see ref 5.

A. Applications in Chemical Reaction Dynamics. The methodology for solving the generalized Born−Oppenheimer equation described above was first applied to the inelastic scattering of $H + O_2(v, j) \rightarrow H + O_2(v', j')$ at low collision energies and zero total angular momentum (i.e., $J = 0$).[11,26,35,36] The ground-state electronic potential energy surface for the HO_2 molecule contains a conical intersection which occurs for T-shaped (C_{2v}) geometries. It also contains two conical intersections which occur for linear geometries. As mentioned in section II, these conical intersections occur along a one-dimensional curve within the three-dimensional nuclear parameter space. The shape and topology of this one-dimensional curve can be quite complicated. It may consist of several branches and/or loops. Specialized electronic structure techniques are often required to accurately map out the shape of this one-dimensional subspace.[56,57] Fortunately, the minimum energy pathway around each of the linear conical intersections in HO_2 exhibits a barrier of about 0.42 eV relative to the asymptotic $H + O_2$ potential well.[58] Thus, for total scattering energies below 0.42 eV, the nuclear motion wave function will not have appreciable amplitude along the entire minimum energy pathway around the linear conical intersections, and the effects of the geometric phase associated with these intersections can be ignored. However, the minimum energy pathway around the C_{2v} conical intersection contains no barrier.[58] Thus, the nuclear motion wave function can have significant amplitude along the entire minimum energy pathway around this intersection even for very low scattering energies near threshold. To quantify the effects of the geometric phase due to the C_{2v} conical intersection, two sets of calculations were performed. One set included the geometric phase by solving the generalized Born−Oppenheimer eq 13. The other set did not include the geometric phase and solved the standard Born−Oppenheimer eq 9. Both sets of calculations implemented single-valued boundary conditions on the nuclear motion wave function. Significant differences between the two sets of calculations were observed. The transition probabilities were computed as a function of total energy. Many of the probabilities which include the geometric phase were found to be shifted in energy (i.e., "out-of-phase") with respect to those which did not include the geometric phase.[26] The geometric phase also lowered the average $J = 0$ cumulative transition probability for the lowest vibrational transition by 35%.[35] Significant differences were also seen in the resonance spectrum. The geometric phase altered many of the resonance energies and lifetimes. In addition, new resonances appeared when the geometric phase was included which were not present in the spectrum calculated without the geometric phase. Similarly, many of the resonances in the spectrum calculated without the geometric phase were missing in the spectrum which included the geometric phase.[26,35] Gauge invariance was also tested by performing a third set of calculations which solved the generalized Born−Oppenheimer eq 13 but with $l = 2$ (see eq 15). The $l = 2$ results do not include geometric phase effects and should be identical to the results based on solving the standard Born−Oppenheimer eq 9 with single-valued boundary conditions (i.e., the $l = 0$ case). As expected, excellent agreement was observed between the $l = 2$ and $l = 0$ calculations for the resonance spectrum and transition probabilities which indicates that the calculations are well converged and that gauge invariance is satisfied.[26,35] In summary, the geometric phase significantly alters the results of the calculations on $H + O_2$ inelastic scattering for $J = 0$ and it must be included in the theoretical treatment in order to obtain the correct results. However, the effects of the geometric phase on physical observables such as integral and differential cross

sections requires calculations for $J > 0$. That is, a separate calculation for each value of J and inversion parity $P = \pm$ are required up to some maximum value of $J = J_{max}$ (where J_{max} is determined from convergence studies). The contributions from each value of J are then added together to obtain fully converged cross sections. To investigate the importance of the geometric phase on fully converged cross sections, the vector potential approach was recently extended to include nonzero total angular momentum. Applications of this method to the $H + H_2$ reaction (and its isotopic variants) will be discussed in Section IV.

B. Applications in Molecular Spectra. The methodology for solving the generalized Born−Oppenheimer equation described above was also used to investigate the effects of the geometric phase on the vibrational states of HO_2 [35] and Na_3 [36,39] for zero total angular momentum (i.e., $J = 0$). The bound state calculations use the same computer codes that are used to compute the surface functions for the scattering calculations. However, the bound state calculations use a renormalized Numerov propagator[59] and an energy bisection algorithm to propagate the coupled-channel radial equations and obtain the vibrational energies and wave functions (see ref 35 for more details). The C_{2v} conical intersection in HO_2 gives rise to a geometric phase which alters the symmetry of the nuclear motion wave function causing it to simultaneously exhibit both even and odd symmetry (with respect to an interchange of the two identical nuclei of ^{16}O).[11,35,60,61] Thus, the correct nuclear motion wave functions exhibit even symmetry across the C_{2v} saddle point and odd symmetry across the C_{2v} symmetry line for $H-O_2$ geometries (see Figure 5 in ref 11). The odd symmetry for $H-O_2$ correlates to the odd rotational levels of O_2 (because of Bose statistics only the odd rotational levels of O_2 are physically allowed).[62] Four sets of bound state calculations for HO_2 were performed. The first set included the geometric phase by solving the generalized Born−Oppenheimer eq 13, the second set ignored geometric phase effects and solved the standard Born−Oppenheimer eq 9 using a single-valued basis set which exhibits even symmetry across the C_{2v} saddle point, the third set also ignored geometric phase effects but used an odd single-valued basis set, and the fourth set tested gauge invariance by solving eq 13 with $l = 2$. For low-lying vibrational states, the vibrational energies for the even and odd states are essentially degenerate. However, for higher-lying states, tunneling across the C_{2v} saddle point gives rise to small energy differences between the even and odd energy levels. For high-lying states, whose energy lies above the C_{2v} saddle point, large differences (up to100 cm^{-1}) between the even and odd energy levels occur. However, even the very high-lying vibrational wave functions remain localized over the deep attractive HO_2 potential well and do not extend along the entire minimum energy pathway around the C_{2v} conical intersection.[35] Thus, the results of calculations which include the geometric phase are identical to those which ignore the geometric phase but use a single-valued basis set which exhibits *even* symmetry across the C_{2v} saddle point.[35] We note that, even though there are no geometric phase effects on the vibrational states of HO_2, the symmetry must be taken into account. The first bound state calculations for HO_2 did not take into account the change in symmetry and computed the wrong states (i.e., those of odd symmetry).[63]

The ground-state electronic potential energy surface for the Na_3 molecule contains a conical intersection which occurs for equilateral triangle (D_{3h}) geometries. Because of the 3-fold symmetry of Na_3, three identical barriers occur along the minimum energy pathway around the conical intersection. These barriers are relatively small so that significant geometric phase effects can occur even for low-lying vibrational states. The geometric phase alters the symmetry of the vibrational wave functions, so that for a given fixed value of the hyper-radius ρ the functions which are even (odd) across the three symmetry lines which bisect the three symmetric potential wells are simultaneously odd (even) across the three symmetry lines which bisect the saddle points between the wells (see Figures 7 and 8 in ref 36). Two sets of bound state calculations for Na_3 were performed. One set included the geometric phase by solving the generalized Born−Oppenheimer eq 13 with $l = 3$, and the other set ignored geometric phase effects and solved the standard Born−Oppenheimer eq 9 using a single-valued basis set. For each set of calculations, the vibrational states of even and odd symmetry (with respect to the symmetry lines which bisect the wells) were computed.[36] As expected, the geometric phase shifted the vibrational energies for many of the vibrational states whose energy lies near or above that of the barriers.[36] The geometric phase causes the vibrational states of even (odd) symmetry to be shifted higher (lower) in energy relative to those which do not include the geometric phase. These energy shifts are due to the fact that the even (odd) vibrational states which include the geometric phase exhibit (do not exhibit) a node across the saddle points, whereas those which do not include the geometric phase do not exhibit (exhibit) a node. The bound state calculations for Na_3 were later extended to include states of E symmetry and the state assignments for the different vibrational modes (i.e., symmetric stretch, asymmetric stretch, and bend).[39] The state assignments showed that the energy shifts which are due to the geometric phase result in a reordering of many of the energy levels (relative to the calculation which ignores geometric phase effects). In particular, the low-lying states of even symmetry (A_1) lie above the states of E symmetry, and the low-lying states of odd symmetry (A_2) lie below the states of E symmetry when the geometric phase is included. The reverse ordering occurs in calculations which ignore the geometric phase. For the very lowest vibrational states, the energy differences between the A_1 and E and the A_2 and E symmetry states are very small so that the reordering due to the geometric phase is difficult to detect. In summary, the geometric phase reorders many of the vibrational energy levels for Na_3 and must be included in the theoretical treatment in order to obtain the correct results. Calculations of the vibrational levels for nonzero total angular momentum using a new and more accurate potential energy surface are currently underway.[64]

IV. Geometric Phase Effects in the $H + H_2$, $H + D_2$, and $D + H_2$ Reactions

Because of its fundamental nature, the H_3 triatomic molecule is an excellent candidate for accurate theoretical and experimental study. In this section, we review some of the past theoretical and experimental studies on the $H + H_2$ reaction system with an emphasis on those related to geometric phase effects. Recent applications of the newly developed vector potential approach to this reaction system are discussed. In sections IVa and IVb, we present new quantum reactive scattering results using this methodology for the $D + H_2$ and $H + H_2$ reactions, respectively.

The H_3 molecule contains a conical intersection which occurs between the ground and first excited electronic states for equilateral (D_{3h}) nuclear geometries. The minimum energy of this intersection is quite high (2.7 eV relative to the bottom of the H_2 well) so that, for low collision energies, the Born−Oppenheimer approximation is valid and the nuclear dynamics

can be accurately calculated using a single (ground state) electronic potential energy surface. However, because of the low potential energy barrier (0.42 eV) between the different nuclear arrangements, the nuclear motion wave function can have significant amplitude along the entire minimum energy pathway around the conical intersection even for relatively low collision energies. Thus, a correct theoretical treatment of the $H + H_2$ reaction (and its isotopic variants) must include geometric phase effects.

The first quantum reactive scattering calculations to include geometric phase effects were reported in 1990 by Lepetit and Kuppermann[32] for the $H + H_2$ system and zero total angular momentum ($J = 0$). They solved the standard Born−Oppenheimer eq 9 and included the geometric phase by implementing double-valued boundary conditions on the nuclear motion wave function. These calculations were later extended to include all $J \leq 34$ to obtain the first fully converged scattering results to include the geometric phase by Wu, Kuppermann, and Lepetit.[33] For para → para and ortho → ortho transitions, the geometric phase was reported to significantly alter the differential cross sections and to a lesser extent, integral cross sections, for total energies of 1.2 eV and below (where direct (nonreactive) processes dominate). Later, these calculations were extended to much higher energies (2.6 eV) in order to investigate the effects of the geometric phase on the para → ortho and ortho → para transitions (i.e., exchange (reactive) processes).[65] Significant geometric phase effects were reported in the rotational distributions and integral cross sections for energies above 1.8 eV.[65]

In 1991, Kliner, Adelmann, and Zare[66] (see also ref 67) performed rotational state distribution measurements for the $D + H_2$ reaction. Significant differences were observed between the experimental results and several quantum reactive scattering calculations[68−70] for $H_2(v = 1, j = 1)$ and a collision energy of 1.0 eV (which corresponds to a total energy of 1.8 eV). The original theoretical calculations ignored geometric phase effects. In 1993, Kuppermann and Wu performed fully converged quantum reactive scattering calculations for the $D + H_2$ reaction which included geometric phase effects.[71] The persistent differences between the experimental results and the original theoretical calculations were reported to be due almost entirely to the geometric phase.[71] Thus, this experiment is often cited as the first experimental measurement of a geometric phase effect in a chemical reaction. Kuppermann and Wu also reported large geometric phase effects in the differential cross sections for a total energy of 1.8 eV but no experimental rotationally resolved differential cross sections were available for comparison. They also reported significant geometric phase effects in the differential cross sections for a total energy of 1.25 eV. However, no geometric phase effects in the integral cross sections were reported at this energy. At 0.78 eV, no geometric phase effects were reported in either the integral or differential cross sections.

Experimental differential cross sections for the $H + D_2$ ($v = 0, j = 0, 1, 2$) → HD + D reaction became available in 1993.[72] In 1995, Wu and Kuppermann[73] pursued calculations for this system and calculated differential cross sections at a total energy of 1.481 eV both with and without the geometric phase. Significant differences between the two sets of calculations were observed, and the calculations which include the geometric phase were reported to be in much better agreement with the experimental results.[73] Additional calculations in the energy range $E_{tot} = 1.42-1.53$ eV showed a pronounced resonance close to 1.481 eV for the $H + D_2$ ($v = j = 0$) → HD ($v' = 0, j' = 4, 5$) + D transitions due entirely to the geometric phase.[74] No resonance was observed when the geometric phase was neglected. In 1997, Wrede and Schnieder[75] attempted to experimentally verify the predicted resonance by performing high-resolution molecular beam experiments in the energy range $E_{tot} = 1.461-1.491$ eV. Surprisingly, they did not see any experimental evidence for the theoretically predicted resonance. Furthermore, their differential cross section for $E_{tot} = 1.481$ eV did not agree with the original experiments of Zare and coworkers[72] or the theoretical results of Wu and Kuppermann[73] which include the geometric phase. In fact, their results are in excellent agreement with theoretical treatments which *do not* include the geometric phase.[52,76−81] Previous experiments by Schnieder et al.[82] at a slightly lower energy $E_{tot} = 1.471$ eV are also in excellent agreement with theoretical calculations which ignore geometric phase effects. The original calculations by Wu and Kuppermann used the LSTH potential energy surface.[83] Unpublished calculations by Wu and Kuppermann for the differential cross section summed over all final vibrational and rotational states at $E_{tot} = 1.481$ eV using the newer BKMP2 surface[84] show no geometric phase effects and are in good agreement with the new experimental results of Wrede and Schnieder.[75] However, there are significant discrepancies in the state resolved differential cross sections computed by Wu and Kuppermann using the BKMP2 surface and the experimental results of Wrede and Schnieder.[75] Furthermore, the state resolved differential cross sections computed by Wu and Kuppermann *without* the geometric phase using either the LSTH or BKMP2 surfaces are significantly different than those computed by several other theoretical groups.[52,76−81] The theoretical results by Wu and Kuppermann which include the geometric phase and use the BKMP2 surface are not consistent with their original calculations using the LSTH surface.[73] This discrepancy has been attributed to subtle differences between the LSTH and BKMP2 surfaces.[75,85] The geometric phase resonance predicted by Wu and Kuppermann is shifted down to 1.442 eV on the BKMP2 surface.[85,86]

Additional experiments were performed at much higher energies ($E_{tot} = 2.391$ eV) and compared to quasiclassical trajectory calculations (which do not include the geometric phase) on the LSTH and the double-many-body-expansion (DMBE) surfaces.[87] Reasonably good agreement between the quasiclassical trajectory results and experiment was found for both of these surfaces. Experiments at an energy of $E_{tot} = 2.86$ eV (i.e., *above* the minimum energy of the conical intersection) have also been performed.[88] These experiments were compared to quasiclassical trajectory calculations on the BKMP2 surface (which omit both the geometric phase and nonadiabatic coupling). Surprisingly good agreement was found between the experimental results and quasiclassical trajectory calculations. Recently, more detailed experimental studies at $E_{tot} = 2.391$ eV have been reported and compared to accurate quantum mechanical calculations (which do not include the geometric phase) on the BKMP2 PES.[89] Excellent agreement between the experimental and quantum mechanical calculations for several state resolved differential cross sections was reported.

In summary, good agreement has been observed between the recent experimental results of Wrede and Schnieder and several theoretical treatments which *do not* include the geometric phase: the quasiclassical trajectory studies at $E_{tot} = 2.391$ and 2.86 eV and especially the quantum mechanical studies at $E_{tot} = 1.481$ and 2.391 eV. This agreement suggests that the effects of the geometric phase are not very important for the $H + D_2$ reaction at all of these energies. The absence of geometric phase

effects was somewhat surprising and motivated additional theoretical calculations. The vector potential approach was recently applied to the H + D_2 reaction.[37] Surprisingly, these calculations showed that the geometric phase effects completely cancel out in all of the state resolved integral and differential cross sections for all energies when the contributions from even and odd values of total angular momentum (J) are added together (for $J \leq 5$). The cancellation occurred for both the LSTH and BKMP2 surfaces and appears to be related to the alternating symmetry of the Wigner D functions with respect to even and odd J. If the cancellation is due to symmetry, then it should be independent of the potential energy surface and should also hold for all J. This would imply that there are no geometric phase effects in the fully converged integral and differential cross sections for all energies and would explain why geometric phase effects have not been seen in any of the experimentally measured state resolved differential cross sections for the H + D_2 reaction. If the cancellation is due to symmetry, then it should also occur for all A + B_2 reactions including the D + H_2 reaction. This would question the validity of the geometric phase results of Kuppermann and Wu for the D + H_2 reaction[71] and also the experimental results of Kliner, Adelmann, and Zare.[66] Kuppermann and Wu[85] have recently published additional results for the H + D_2 reaction based on both the LSTH and BKMP2 surfaces and have claimed that the cancellation of geometric phase effects does not hold for all J. However, their state resolved differential cross sections *without* the geometric phase using either the LSTH or BKMP2 surfaces still do not agree with the experimental results of Wrede and Schnieder[75] or the results of several other theoretical groups.[52,76−81] Thus, it appears that there may be errors in the calculations by Kuppermann and Wu which need to be resolved. A possible explanation for these discrepancies was suggested in 1999.[50] In body-frame symmetrized hyperspherical coordinates, an Eckart singularity occurs at the north pole ($\theta = 0$) and the another one occurs at the equator ($\theta = \pi/2$) (see ref 50 for details). Our reactive scattering calculations use a basis set and methodology which accurately treats *both* of these singularities.[37,52] However, the methodology which is used by Kuppermann and Wu is not capable of treating both of these singularities. Significant errors can occur even for low collision energies if the Eckart singularities are not properly treated. A proper treatment of these singularities requires the introduction of double-valued functions of the hyperangle ϕ and the use of Jacobi polynomials in the hyperangle θ.[50]

A. Quantum Reactive Scattering Calculations for the D + H_2 → HD + H Reaction. In this section, we report the results of accurate quantum reactive scattering calculations for the D + H_2 (v, j) → HD (v', j') + H reaction at 48 values of total energy in the range 0.4−2.32 eV. The calculations are based on the same numerical parameters and basis sets that were used in previous calculations on the H + D_2 reaction.[52] Reaction probabilities, integral, and differential cross sections are computed using the BKMP2 potential energy surface for all values of total angular momentum $J \leq 19$. The calculations are performed both with and without the geometric phase. The geometric phase calculations are done using two different methods. One method uses the vector potential approach which is based on solving the generalized Born−Oppenheimer eq 13 with single-valued boundary conditions. The second method uses the double-valued basis set approach which is based on solving the standard Born−Oppenheimer eq 9 with double-valued boundary conditions. As expected, these two methods give identical results.

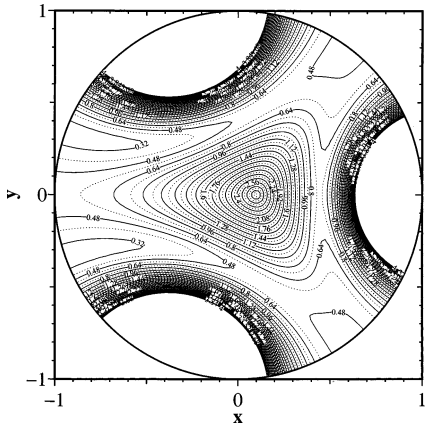

Figure 2. Contour plot of the DH_2 potential energy surface with the hyper-radius ρ fixed at 3.27 a_0. This plot is a stereographic projection of the surface of an upper half-sphere. The hyperangle θ runs from 0 at the north pole ($x = 0$, $y = 0$) to $\pi/2$ at the equator (heavy circle). The hyperangle ϕ, the azimuthal angle, is measured from the positive x axis and goes to π in the counterclockwise direction and to $-\pi$ in the clockwise direction. The contours start at 0.32 eV and end at 4.0 eV. The spacing between the dark contours is 0.16 eV with a dashed contour halfway between. All energies are relative to the bottom of the H_2 potential well. The conical intersection is clearly visible just to the right of the origin.

Figure 2 is a contour plot of the BKMP2 potential energy surface for DH_2 at $\rho = 3.27$ a_0. The D_{3h} conical intersection is clearly visible just to the right of the origin. Because we are using *mass-scaled* symmetrized hyperspherical coordinates, the D_{3h} conical intersection is *not* located at the origin of our coordinate system. The conical intersection is located at $\theta = 11.537°$ and $\phi = 0$ which corresponds to ($x \approx 0.1$, $y = 0$). Its location in (θ, ϕ) space is independent of the hyper-radius ρ. Figure 2 shows that the minimum energy pathway around the conical intersection for $\rho = 3.27$ a_0 contains a barrier of about 0.55 eV which occurs for ($x = -1$, $y = 0$), a barrier of about 0.71 eV which occurs for ($x = 0.45$, $y = 0$), and two barriers of about 0.51 eV each which occur for ($x = 0.18$, $y = \pm 0.5$). The heights of these barriers vary with ρ. As ρ is decreased from 3.27 a_0, the barrier at $x = -1$ decreases toward its minimum value (0.42 eV), the barriers at $x = 0.18$ disappear, and the barrier at $x = 0.45$ increases. As ρ is increased from 3.27 a_0, the barrier at $x = -1$ increases, the barrier at $x = 0.45$ disappears, and the barriers at $x = 0.18$ decrease toward their minimum values (0.42 eV) and move to linear geometries (the equator) at $x \approx 0.63$.

Because the nuclei of the two H atoms in DH_2 are spin-1/2 fermions,[62] the total molecular wave function (Ψ_{tot} of eq 8) must be antisymmetric under a permutation ($\mathscr{P}$) of the two identical nuclei. Because the nuclear spin is $S = 1/2$, we have a total of $(2S + 1)^2 = 4$ nuclear spin states with $(2S + 1)(S + 1) = 3$ being symmetric and $(2S + 1)S = 1$ being antisymmetric. The symmetric states have the larger statistical weight and are called *ortho*-H_2. The antisymmetric states are called *para*-H_2. Because the ground electronic state of H_2 is a $^1\Sigma_g^+$ state,[90] we know that asymptotically (i.e., for large ρ) the electronic wave function for D−H_2 is symmetric. Because the total wave function must be antisymmetric and the electronic wave function is symmetric, we know that for *ortho* (*para*)-H_2 the nuclear motion wave function (Ψ) must be antisymmetric (symmetric) for D−H_2. Thus, for *ortho* (*para*)-H_2 the nuclear motion wave function is antisymmetric (symmetric) across the x axis to the right of the conical intersection (i.e., for $x > 0.1$) in Figure 2. The nuclear motion wave functions for large ρ and $x > 0.1$ correlate to the rovibrational states of the H_2 diatomic molecule. For *ortho*

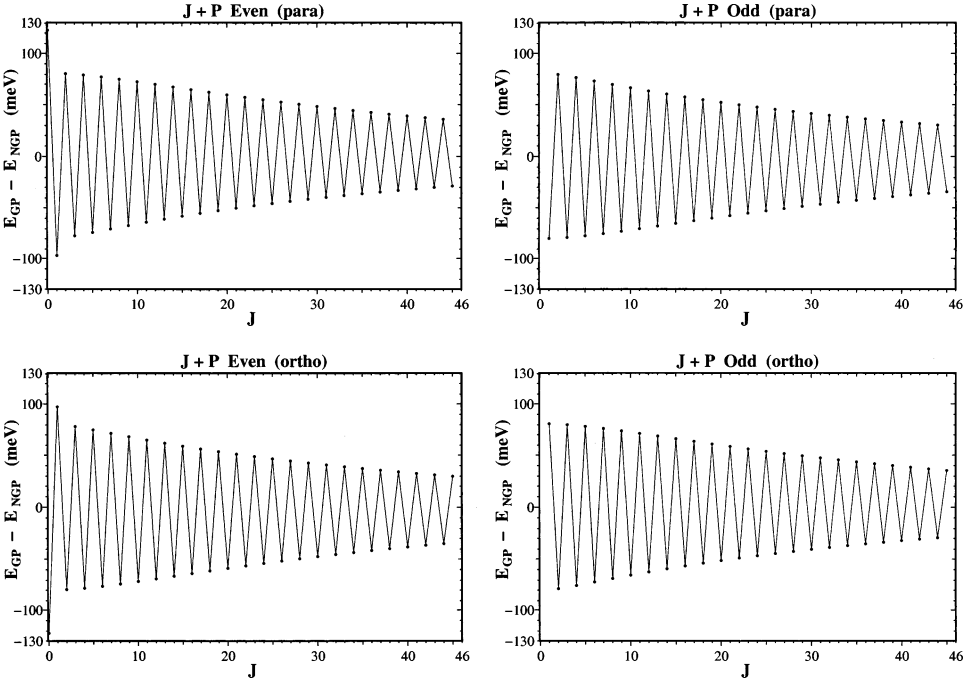

Figure 3. Difference between the lowest surface function energy which includes the geometric phase (denoted by E_{GP}) and that which does not (denoted by E_{NGP}) is plotted as a function of total angular momentum J and inversion parity P for both *ortho*- and *para*-H_2. The calculations are at a fixed hyper-radius of $\rho = 2.96\ a_0$. The data points are connected by line segments to help guide the eye.

(*para*)-H_2, only the odd (even) rotational levels of H_2 are compatible with Fermi statistics. The geometric phase alters the symmetry of the real electronic wave function for DH_2 so that it is antisymmetric across the x axis to the left of the conical intersection (i.e., for $x < 0.1$) in Figure 2. This change in symmetry is a direct consequence of the wave function's double-valuedness (see eq 11 and ref 60). Thus, in order for the total molecular wave function to satisfy Fermi statistics for all nuclear geometries, for *ortho* (*para*)-H_2, the nuclear motion wave function must be symmetric (antisymmetric) across the x axis to the left of the conical intersection (i.e., for $x < 0.1$) in Figure 2.

Figure 3 plots the difference between the lowest surface function energy computed with and without the geometric phase at $\rho = 2.96\ a_0$ as a function of total angular momentum J and inversion parity $P = \pm$. The surface function energies which include the geometric phase were computed using both the vector potential approach and the double-valued basis set approach. As expected, both methods produce essentially identical low-lying surface function energies. The upper (lower) two plots are for *para* (*ortho*)-H_2. For all cases, the energy differences alternate sign with respect to even and odd J, and the magnitude of the energy differences decreases with increasing J. The alternating sign of the energy differences can be traced to the alternating symmetry of the Wigner D functions. For example, for $J = 0$, 1, and even parity ($P = +$), the properly symmetrized nuclear motion wave function can be expressed in the following way[37,50]

$$\Psi_i^{JMPq=\pm} = \frac{1}{\sqrt{2}}[e^{il\eta/2}\,\psi_i^{JP}(\rho, \theta, \phi) \pm (-1)^J e^{-il\eta/2}\,\psi_i^{JP}(\rho, \theta, -\phi)]\,\tilde{D}^J_{0M}(\alpha, \beta, \gamma) \quad (19)$$

where the normalized Wigner $\tilde{D}^J_{0M}$ functions are symmetric or antisymmetric under an interchange of the two identical nuclei for even or odd J, respectively. A proper treatment of the geometric phase requires the introduction of the phase factor $\exp(il\eta/2)$ where l is an odd integer. Ignoring the geometric phase corresponds to setting $l = 0$. This phase factor alters the symmetry of the nuclear motion wave function across the x axis to the left of the conical intersection (i.e., for $x < 0.1$) in Figure 2. For $J = 0^+$, the part of the nuclear motion wave function which is in brackets in eq 19 is symmetric for $q = +$ (the upper sign), or antisymmetric for $q = -$ (the lower sign) for $D-H_2$.[50] For $J = 1^+$, the symmetries are reversed. Thus, for $J = 0^+$ and *para*-H_2, we must choose $q = +$ in eq 19 so that the overall nuclear motion wave function (Ψ^{JMPq}) is symmetric asymptotically (i.e., for $D-H_2$). When the geometric phase is ignored, the nuclear motion wave function (Ψ^{JMPq}) is symmetric across the x axis both to the right (i.e., for $x > 0.1$) and left (i.e., for $x < 0.1$) of the conical intersection. However, when the geometric phase is included, the nuclear motion wave function is symmetric to the right and antisymmetric to the left of the conical intersection. For $\rho = 2.96\ a_0$, the antisymmetry corresponds to a node in the wave function which occurs across the barrier located at ($x = -1$, $y = 0$) (see Figure 2). This node shifts the surface function energy higher relative to the purely symmetric case which ignores the geometric phase. Thus, the energy difference $E_{GP} - E_{NGP}$ is positive (see Figure 3). For $J = 1^+$ and *para*-H_2, we must still choose $q = +$ in eq 19 so that the overall nuclear motion wave function (Ψ^{JMPq}) is symmetric asymptotically (i.e., for $D-H_2$). For this case, the normalized Wigner $\tilde{D}^1_{0M}$ functions are antisymmetric. When the geometric phase is ignored, the part of the nuclear motion wave function which is in brackets in eq 19 is antisymmetric to the right and left of the conical intersection. However, when the geometric phase is included, the part of the nuclear motion wave function which is in brackets in eq 19 is antisymmetric to the right and symmetric to the left of the conical intersection. The node in the antisymmetric surface function which ignores the geometric phase occurs across the barrier located at ($x = -1$, $y = 0$) and causes the energies to lie higher relative to the symmetric surface function which includes the geometric phase. Thus, the energy difference $E_{GP} - E_{NGP}$ is negative (see Figure 3). For *ortho*-

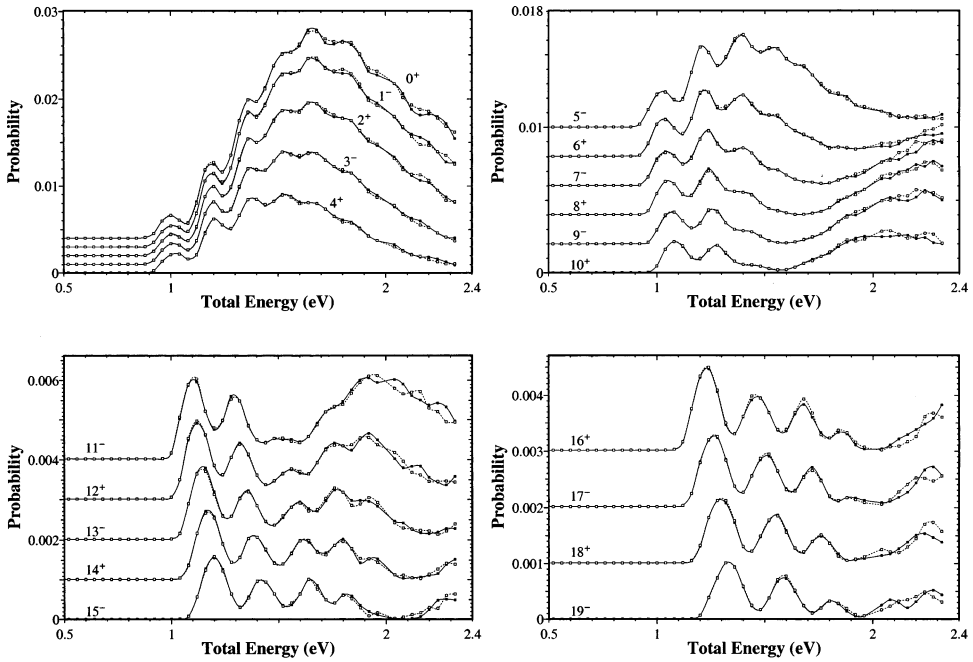

Figure 4. Reaction probabilities for D + H_2 ($v = 1$, $j = 0$) → HD ($v' = 0$, $j' = 0$) + H are plotted as a function of total energy for all values of $J \leq 19$. The solid curves and data points do not include the geometric phase. The short dashed curves and open squares include the geometric phase and are based on the vector potential approach which accurately treats the location of the conical intersection. The numbers labeling each set of curves denote the value of J^P. The curves are shifted to make viewing easier. The flat part of the curves near 0.5 eV corresponds to zero probability and indicates the value of the shift. The data points are calculated values and the curves are a cubic spline fit.

H_2, we must choose $q = -$, and all of the above symmetry arguments and energy shifts are reversed (see Figure 3). The alternating sign of the energy differences in Figure 3 also occurs for all of the other values of ρ within the interaction region $2.2 \leq \rho \leq 3.45\ a_0$.

The state-to-state reaction probabilities are given by

$$P^{JP}_{vj,v'j'} = \frac{1}{N^{JP}_j} \sum_l \sum_{l'} |S^{JP}_{vjl,v'j'l'}|^2 \tag{20}$$

where N^{JP}_j denotes the number of initial orbital angular momentum l for a given J, P, and j. We note that the sums over l and l' in eq 20 are chosen to be consistent with the identity $P = j + l = j' + l'$. The scattering matrix element $S^{JP}_{vjl,v'j'l'}$ is the appropriately symmetrized scattering matrix element from the initial channel (vjl) to the final channel ($v'j'l'$). For A + B_2 systems, we can choose $S^{JP}_{vjl,v'j'l'} \equiv \sqrt{2}\ S^{JP}_{\tau=1vjl,\tau'=2v'j'l'}$.[91]

Figure 4 plots the reaction probabilities for D + H_2 ($v = 1$, $j = 0$) → HD ($v' = 0$, $j' = 0$) + H as a function of total energy for all $J \leq 19$. We note that, for zero initial rotational angular momentum (i.e., $j = 0$), the only nonzero reaction probabilities are for even $J + P$. The solid curves and data points do not include the geometric phase. The short dashed curves and open squares include the geometric phase and are based on the vector potential approach which accurately treats the location of the conical intersection. At high energies, significant "out-of-phase" behavior occurs between the results which include the geometric and those which do not. The "out-of-phase" behavior alternates "phase" with respect to even and odd J. For example, compare the solid and dashed curves for $J = 0-3$ near 2.15 eV. For $J = 0$, the dashed curve is above the solid curve, and for $J = 1$, the dashed curve is below the solid curve. Similar behavior occurs for $J = 2$ and 3. More alternating "out-of-phase" behavior can be seen for other energies and values of J (especially for $E_{tot} > 1.9$ eV and $J \geq 16$). The alternating "out-of-phase" behavior in the reaction probabilities appears to be related to the alternating symmetry of the Wigner D functions with respect to even and odd J. We have recently extended the calculations to include all $J \leq 34$ and have verified that the "out-of-phase" behavior continues to hold for all of these higher values of J as well.[38]

The differential cross sections for the D + H_2 reaction are given by

$$\frac{d\sigma}{d\Omega}|_{vjm \to v'j'm'} = \frac{\bar{k}_{v'j'}}{\bar{k}_{vj}} |f^{R}_{vjm \to v'j'm'}|^2 \tag{21}$$

where the reactive scattering amplitude is given by

$$f^{R}_{vjm \to v'j'm'} = \sqrt{2}\, f^{\tau=1,\tau'=2}_{vjm \to v'j'm'}(\bar{k}_{vj}, \bar{k}_{v'j'}, \theta_S)$$

and

$$f^{\tau,\tau'}_{vjm \to v'j'm'}(\bar{k}_{vj}, \bar{k}_{v'j'}, \theta_S) = \frac{2\pi}{(\bar{k}_{vj}\bar{k}_{v'j'})^{1/2}} \sum_{Jll'} i^{l-l'+1}\, C(jlJ; m, 0, m)\, C(j'l'J; m', m - m', m) \sqrt{\frac{2l+1}{4\pi}}\, Y_{l'm-m'}(\theta_S, \phi_S)\, T^{J}_{\tau vjl,\tau' v'j'l'} \tag{22}$$

where the $\mathbf{T}$ matrix is defined as $\mathbf{T} = \mathbf{I} - \mathbf{S}$ and $\mathbf{S}$ is the scattering matrix. The magnitude of the wave vector $\bar{\mathbf{k}}_{vj}$ is given by $\bar{k}_{vj} = a\, k_{vj}$ where $a^2 = 2[m_D/(m_D + 2\ m_H)]^{1/2}$, $k^2_{vj} = 2\mu(E_{tot} - \epsilon_{vj})/\hbar^2$, E_{tot} is the total energy, ϵ_{vj} are the diatomic rovibrational energies of H_2, and $\mu = [m_D\ m_H\ m_H/(m_D + 2\ m_H)]^{1/2}$ is the three-body reduced mass. We have chosen the direction of the initial $\mathbf{k}_{vj}$ vector to lie along the space frame z axis so that $M = m$.[44] The polar angles θ_S and ϕ_S define the direction of the center-of-mass velocity vector of the final HD molecule relative to the center-of-mass velocity vector of the initial D atom. Thus, $\theta_S = 180°$ and 0° correspond to backward and forward scattering, respectively. We note that the sums over l

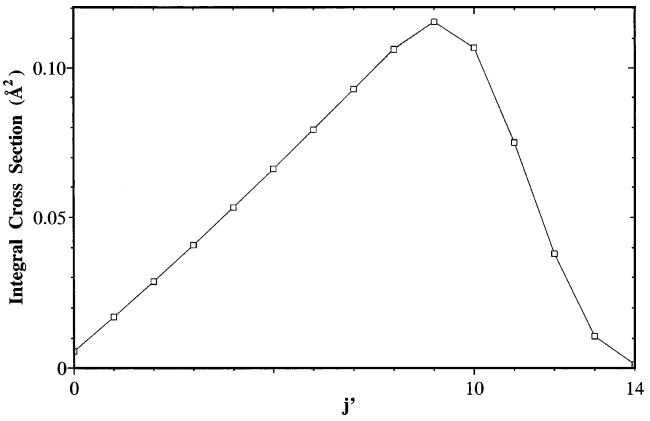

Figure 5. Degeneracy averaged rotational distribution is plotted for $D + H_2$ ($v = 1, j = 1$) → HD ($v' = 1, j'$) + H at $E_{tot} = 1.8$ eV summed over all $J \leq 19$. Two curves are plotted. The solid curve and data points do not include the geometric phase. The short dashed curve and open squares include the geometric phase and are based on the vector potential approach which accurately treats the location of the conical intersection. The geometric phase results lie directly on top of the results which ignore the geometric phase.

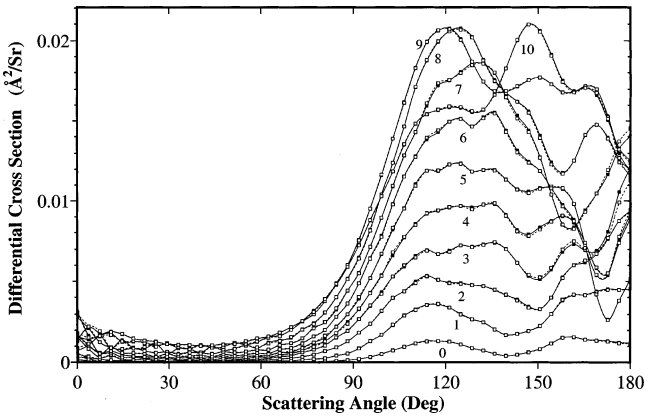

Figure 6. Degeneracy averaged differential cross sections are plotted for $D + H_2$ ($v = 1, j = 1$) → HD ($v' = 1, j'$) + H at $E_{tot} = 1.8$ eV summed over all $J \leq 19$. The number next to each curve labels the value of j'. The solid curves and data points do not include the geometric phase. The short dashed curves and open squares include the geometric phase and are based on the vector potential approach which accurately treats the location of the conical intersection. The geometric phase results are almost identical to the results which ignore the geometric phase.

and l' in eq 22 average out the ϕ_S dependence so that f is a function of θ_S only. The degeneracy averaged cross sections are given by

$$\left.\frac{d\sigma}{d\Omega}\right|_{vj\rightarrow v'j'} = \frac{1}{2j+1}\sum_{m}\sum_{m'}\left.\frac{d\sigma}{d\Omega}\right|_{vjm\rightarrow v'j'm'} \quad (23)$$

Figures 5 and 6 plot the degeneracy averaged rotational distribution and differential cross sections for $D + H_2$ ($v = 1$, $j = 1$) → HD ($v' = 1, j'$) + H at $E_{tot} = 1.8$ eV summed over all values of $J \leq 19$, respectively. The integral cross sections in Figure 5 are computed by numerically integrating eq 23 over the solid angle $d\Omega$. There are two sets of curves in Figures 5 and 6. The solid curves and data points do not include the geometric phase. The short dashed curves and open squares include the geometric phase and are based on the vector potential approach. In both figures, the results which include the geometric phase are essentially identical to those which do not include the geometric phase. Figures 5 and 6 show that all of the geometric phase effects cancel out in both the integral and differential cross sections when the contributions from even and odd values of J are added together (see also Figures 9−15 of ref 37). The cancellation of geometric phase effects in both the integral and differential cross sections with respect to the sum over J occurs for all of the energies and all of the initial and final states that we have looked at. The results in Figures 5 and 6 are not fully converged with respect to the sum over J in eq 22. However, we have recently extended the calculations to include all $J \leq 34$ and have verified that the cancellation continues to hold for fully converged integral and differential cross sections.[38]

Figures 4−6 and the recent calculations[38] which include all $J \leq 34$ confirm the conclusions of ref 37 which claim that the cancellation of geometric phase effects in the integral and differential cross sections should continue to hold for higher values of J. These conclusions are not consistent with the geometric phase calculations of Kuppermann and Wu which predict large geometric phase effects in the fully converged integral and differential cross sections for the $D + H_2$ and $H + D_2$ reactions (see the discussion at the beginning of section IV). However, as noted above, the state resolved differential cross sections computed by Kuppermann and Wu for $H + D_2$ which *do not* include the geometric phase are significantly different than those computed by several other theoretical groups and the recent high-resolution molecular beam experiments. In contrast, our state resolved differential cross sections for $H + D_2$ which *do not* include the geometric phase are in excellent agreement with the results of the other theoretical groups and the recent high-resolution molecular beam experiments.[52] Our double-valued basis set approach for including the geometric phase uses the same computer codes that were used in the calculations for $H + D_2$ which *do not* include the geometric phase.[52] The only difference is one line of code which replaces the basis set $\exp(im\phi)$ with $\exp(i(m + 1/2)\phi)$. This change is so trivial that it seems unlikely that a mistake could be made. Furthermore, our geometric phase results based on the vector potential approach are in excellent agreement with those based on our double-valued basis set approach. Thus, we are confident that all of our geometric phase calculations are correct. Our geometric phase results for the $D + H_2$ reaction also question the validity of the experimental results of Kliner, Adelmann, and Zare[66] which are reported to be in agreement with the geometric phase calculations of Kuppermann and Wu.[71] However, the rotational distribution for $D + H_2$ ($v = 1$, $j = 1$) → HD ($v' = 1, j'$) + H at $E_{tot} = 1.8$ eV was not directly measured experimentally. It was determined by subtracting two other experimentally measured rotational distributions. This procedure makes several assumptions and is prone to errors. Furthermore, this experiment has not yet been confirmed. Clearly, a high-resolution molecular beam experiment for the $D + H_2$ reaction at 1.8 eV is needed in order to resolve the remaining discrepancies between theory and experiment.

B. Quantum Reactive Scattering Calculations for the H + H_2 Reaction. In this section, we report the results of accurate quantum reactive scattering calculations for the $H + H_2$ (v, j) → H_2 (v', j') + H reaction at 96 values of total energy in the range 0.5−2.42 eV. The calculations are based on the same numerical parameters and basis sets that were used in previous calculations on the $H + D_2$ and $D + H_2$ reactions.[38,52] Reaction probabilities, integral, and differential cross sections are computed using the BKMP2 potential energy surface for all values of total angular momentum $J \leq 10$. The calculations are performed both with and without the geometric phase. The

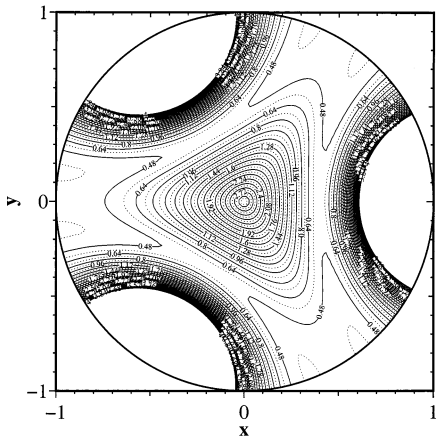

Figure 7. Contour plot of the H_3 potential energy surface with the hyper-radius ρ fixed at 3.27 a_0. This plot is similar to Figure 2 except that the contours start at 0.4 eV and the conical intersection occurs at the origin.

geometric phase calculations are done using two different methods. One method uses the vector potential approach which is based on solving the generalized Born−Oppenheimer eq 13 with single-valued boundary conditions. The second method uses the double-valued basis set approach which is based on solving the standard Born−Oppenheimer eq 9 with double-valued boundary conditions. As expected, these two methods give identical results.

Figure 7 is a contour plot of the BKMP2 potential energy surface for H_3 at $\rho = 3.27\ a_0$. The D_{3h} conical intersection is clearly visible at the origin of the plot $\theta = 0$ (i.e., $x = 0$, $y = 0$). Its location in (θ, ϕ) space is independent of the hyper-radius ρ. Figure 7 shows that the minimum energy pathway around the conical intersection for $\rho = 3.27\ a_0$ contains three barriers of about 0.42 eV each which occur at $(x = -1, y = 0)$ and $(x \approx 0.5, y = \pm 0.86)$ and three barriers of about 0.53 eV each which occur at $(x = 0.4, y = 0)$ and $(x \approx -0.2, y = \pm 0.35)$. The heights of these barriers vary with ρ. As ρ is increased or decreased from 3.27 a_0, the three barriers at $(x = -1, y = 0)$ and $(x \approx 0.5, y = \pm 0.86)$ increase. As ρ is increased from 3.27 a_0, the three barriers at $(x = 0.4, y = 0)$ and $(x \approx -0.2, y = \pm 0.35)$ decrease and eventually disappear. As ρ is decreased from 3.27 a_0, these three barriers increase.

Because the nuclei in H_3 are spin 1/2 fermions,[62] the total molecular wave function (Ψ_{tot} of eq 8) must be antisymmetric under a permutation ($\mathscr{P}$) of any two identical nuclei. Because the nuclear spin is $S = 1/2$, we have a total of $(2S + 1)^3 = 8$ nuclear spin states. Because of the 3-fold symmetry of H_3, the nuclear spin states can be classified using the irreducible representations of the permutation group S_3. The irreducible representations of S_3 are A_1 (symmetric), A_2 (antisymmetric), and E (doubly degenerate). The number of spin states of A_1, A_2, and E symmetry are given by $(2S + 1)(2S + 3)(S + 1)/3 = 4$, $(2S + 1)(2S - 1)S/3 = 0$, and $(2S + 1)(S + 1)8S/3 = 4$, respectively.[36,92] Because the E representation is two-dimensional, there are two distinct spin states of E symmetry, and each one consists of two components which makes a total of four. The two components in each spin state are labeled by $\pm m_s$ (the z component of the total nuclear spin). The nuclear motion wave function (Ψ) can also be classified using the irreducible representations of the permutation group S_3. Because the ground state of H_2 is a $^1\Sigma_g^+$ state,[90] we know that asymptotically (i.e., for large ρ) the electronic wave function for $H-H_2$ is symmetric. Thus, for the A_1 (symmetric) nuclear spin states, we must choose the nuclear motion wave function (Ψ) to be of A_2 symmetry (i.e., antisymmetric) for $H-H_2$ so that the total wave function is antisymmetric. Similarly, for the E nuclear spin states, we must choose the nuclear motion wave function (Ψ) to be of E symmetry for $H-H_2$. The two distinct nuclear spin states of E symmetry combine with each doubly degenerate nuclear motion wave function of E symmetry to form two symmetric and two antisymmetric functions. Only the two antisymmetric functions are physically allowed. Because the real electronic wave function for H_3 is symmetric for $H-H_2$, we know that it is symmetric across the x axis for $x > 0$ (i.e., to the right of the conical intersection in Figure 7). It is also symmetric across the two symmetry lines which extend radially outward from the origin at $\phi = \pm 120°$. The geometric phase alters the symmetry of the real electronic wave function for H_3 so that it is also antisymmetric across the x axis for $x < 0$ (i.e., to the left of the conical intersection in Figure 7). It is also antisymmetric across the two symmetry lines which extend radially outward from the origin at $\phi = \pm 60°$. The antisymmetric behavior is a direct consequence of the wave function's double-valuedness (see eq 11 and refs 36 and 60). To satisfy Fermi statistics for all nuclear geometries, the product of the nuclear motion wave function and nuclear spin wave function must also be double-valued and be antisymmetric across the x axis for $x > 0$ and the two symmetry lines at $\phi = \pm 120°$ and be symmetric across the x axis for $x < 0$ and the two symmetry lines at $\phi = \pm 60°$.

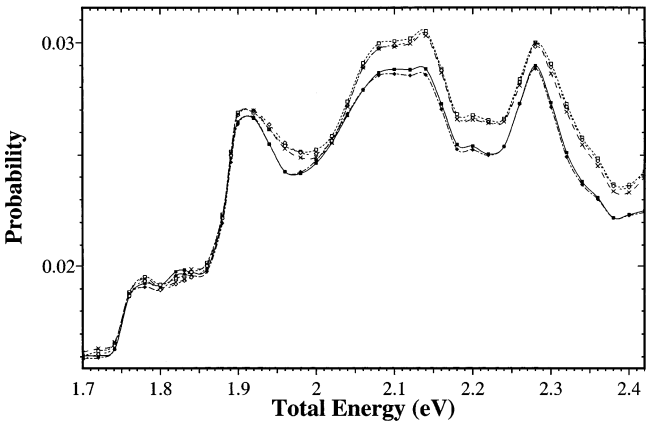

Figure 8. Reaction probability for $H + H_2$ ($v = 0$, $j = 1$) → H_2 ($v' = 1$, $j' = 2$) + H and zero total angular momentum ($J = 0$) is plotted as a function of energy. The solid curve and solid squares do not include the geometric phase. The short dashed curve and open squares include the geometric phase and are based on the vector potential approach with $l = 3/2$. The short dashed curve and open triangles also include the geometric phase and are based on the vector potential approach but are computed with $l = 9/2$. The long dashed curve and Xs also include the geometric phase but are based on the double-valued basis set approach. The short−long dashed curve and solid triangles do not include the geometric phase but are computed using the vector potential approach with $l = 6/2$. The data points are calculated values and the curves are a cubic spline fit.

Figure 8 plots the reaction probability for $H + H_2$ ($v = 0$, $j = 1$) → H_2($v' = 1$, $j' = 2$) + H and zero total angular momentum ($J = 0$) as a function of total energy. The reaction probabilities are computed using eq 20 with $S^{JP}_{v'j'l',vjl} \equiv \sqrt{2}\, S^{JP}_{\tau=1vjl,\tau'=2v'j'l'}$. Significant differences occur between the results which include the geometric phase (the solid curve and squares) and those which do not (the dashed curve and open squares) for energies above about 1.9 eV. The dashed curve and open squares include the geometric phase and are based on the vector potential approach with $l = 3/2$. The long-dashed curve and X's also include the geometric phase but are based on the double-valued basis set approach. The double-valued basis set approach uses the same computer codes that were used in the

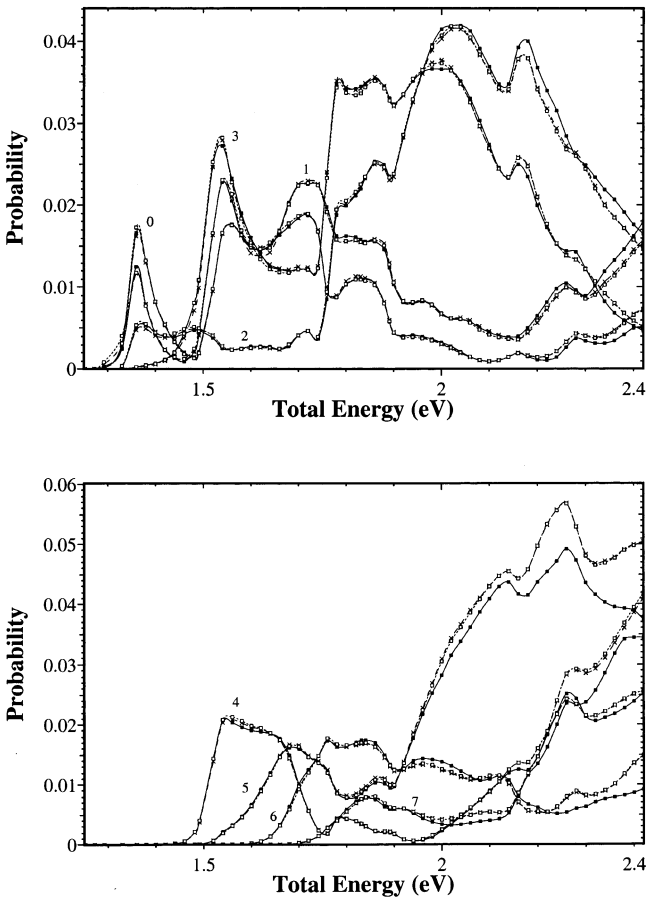

Figure 9. Reaction probabilities for H + H_2 ($v = 1, j = 0$) → H_2 ($v' = 2, j'$) + H and zero total angular momentum ($J = 0$) are plotted as a function of energy. The solid curve and solid squares do not include the geometric phase. The short dashed curve and open squares include the geometric phase and are based on the vector potential approach with $l = 3/2$. The long dashed curve and Xs also include the geometric phase but are based on the double-valued basis set approach. The number next to each set of curves labels the value of j'. The data points are calculated values, and the curves are a cubic spline fit.

calculations which *do not* include the geometric phase. The only difference is one line of code which replaces the basis set $\exp(im\phi)$ with $\exp(i(m + 3/2)\phi)$. As expected, the results based on the double-valued basis set approach are in good agreement with those based on the vector potential approach. Gauge invariance is also verified by performing the calculations using the vector potential approach but with $l = 9/2$ and $l = 6/2$. The $l = 9/2$ results are related to those with $l = 3/2$ by a gauge transformation.[7,19] The dashed curve and open triangles in Figure 8 are the results using $l = 9/2$. As expected, good agreement is observed between the $l = 9/2$ and $l = 3/2$ reaction probabilities. The small differences are due to numerical convergence errors. The $l = 6/2$ results are related to those with $l = 0$ by a gauge transformation and correspond to doing the calculations without the geometric phase. The short−long dashed curve and solid triangles in Figure 8 are the results using $l = 6/2$. As expected, good agreement is observed between the $l = 6/2$ and $l = 0$ reaction probabilities. Gauge invariance and the good agreement between the double-valued basis set approach and the vector potential approach are also observed for other initial and final states and nonzero values of J.

Figure 9 plots the reaction probabilities for H + H_2 ($v = 1$, $j = 0$) → H_2($v' = 2, j'$) + H and zero total angular momentum ($J = 0$) as a function of total energy. Significant differences occur between the results which include the geometric phase (the solid curves and squares) and those which do not (the dashed curves and open squares) for energies above about 1.9 eV. The most notable differences occur for $j' = 5$ at high energies. The long-dashed curves and Xs also include the geometric phase but are based on the double-valued basis set approach. As expected, the results based on the double-valued basis set approach are in good agreement with those based on the vector potential approach.

The physically measurable cross sections for the H + H_2 reaction are obtained from wave functions which have been properly antisymmetrized with respect to an interchange of any two nuclei (see the above discussion on symmetry). This can be done by the technique of postantisymmetrization. That is, the cross sections are computed as if the atoms were distinguishable. The distinguishable atom cross sections are then properly antisymmeterized to obtain the physical ones.[91,93−95] The relevant expressions for the physically measurable differential cross sections are given by

$$\left.\frac{d\sigma}{d\Omega}\right|_{vjm\rightarrow v'j'm'} = \frac{\bar{k}_{v'j'}}{\bar{k}_{vj}}|f^{N}_{vjm\rightarrow v'j'm'} - (-1)^{i_{gp}} f^{R}_{vjm\rightarrow v'j'm'}|^2, \quad (24)$$

for j and j' even (i.e., para → para)

$$\left.\frac{d\sigma}{d\Omega}\right|_{vjm\rightarrow v'j'm'} = \frac{\bar{k}_{v'j'}}{\bar{k}_{vj}} 3|f^{R}_{vjm\rightarrow v'j'm'}|^2 \quad (25)$$

for j even and j' odd (i.e., para → ortho)

$$\left.\frac{d\sigma}{d\Omega}\right|_{vjm\rightarrow v'j'm'} = \frac{\bar{k}_{v'j'}}{\bar{k}_{vj}}|f^{R}_{vjm\rightarrow v'j'm'}|^2 \quad (26)$$

for j odd and j' even (i.e., ortho → para), and

$$\left.\frac{d\sigma}{d\Omega}\right|_{vjm\rightarrow v'j'm'} = \frac{\bar{k}_{v'j'}}{\bar{k}_{vj}}[|f^{N}_{vjmf\rightarrow v'j'm'} + (-1)^{i_{gp}} f^{R}_{vjm\rightarrow v'j'm'}|^2 + 2|f^{R}_{vjm\rightarrow v'j'm'}|^2] \quad (27)$$

for j and j' odd (i.e., ortho → ortho), where f^R and f^N denote the reactive and nonreactive scattering amplitudes, respectively. The reactive scattering amplitude is given by $f^R = f^{\tau=1,\tau'=2}_{vjm\rightarrow v'j'm'}(\bar{k}, \bar{k}', \theta_S)$, and $f^{\tau,\tau'}_{vjm\rightarrow v'j'm'}$ is given by eq 22. Similarly, the nonreactive scattering amplitude is given by $f^N = f^{\tau=1,\tau'=1}_{vjm\rightarrow v'j'm'}(\bar{k}, \bar{k}', \theta_S)$. The scattering angle θ_S denotes the direction of the center-of-mass velocity vector of the final H_2 molecule relative to the center-of-mass velocity vector of the initial H atom. Thus, $\theta_S = 180°$ and 0° correspond to backward and forward scattering, respectively. The magnitude of the wave vector $\bar{\mathbf{k}}_{vj}$ is given by $\bar{k}_{vj} = a\, k_{vj}$ where $a^2 = 2/\sqrt{3}$, $k^2_{vj} = 2\,\mu\,(E_{tot} - \epsilon_{vj})/\hbar^2$, E_{tot} is the total energy, ϵ_{vj} are the diatomic rovibrational energies of H_2, and μ is the three-body reduced mass $\mu = m_H/\sqrt{3}$. The sign $(-1)^{i_{gp}}$ changes the sign of the interference terms between the reactive and nonreactive contributions to eqs 24 and 27 depending upon whether the geometric phase is included ($i_{gp} = 1$) or not ($i_{gp} = 0$). This sign factor is a direct consequence of the double-valuedness of the real electronic wave function which changes sign under a cyclic permutation of the three identical nuclei.[8]

Figure 10 plots the degeneracy averaged partial integral cross sections for the H + H_2 ($v = 0, j = 0$) → H_2 ($v' = 1, j' = 0-3$) + H reaction as a function of total energy. These cross sections include all $J \leq 10$ and are computed by numerically integrating

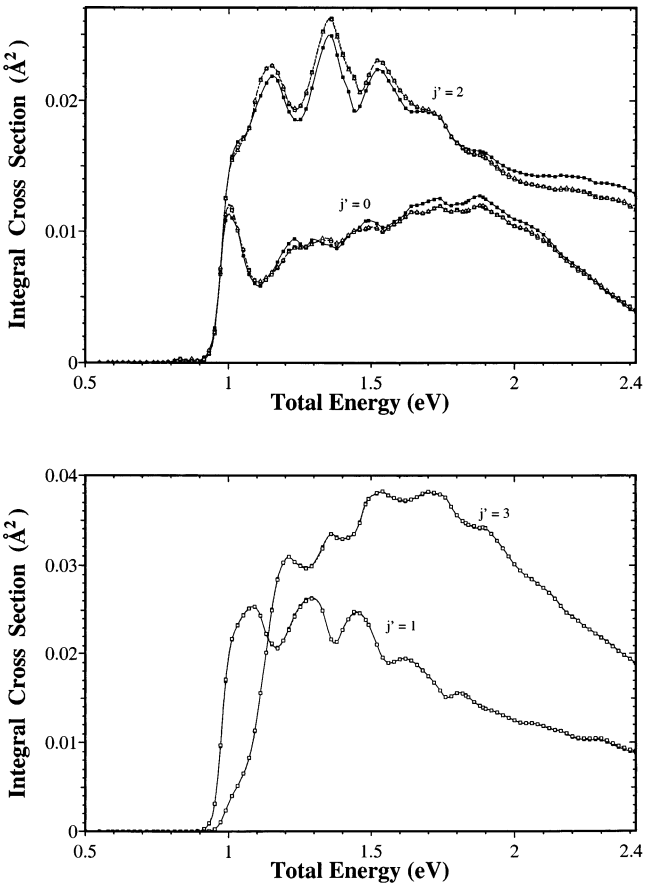

Figure 10. Degeneracy averaged partial integral cross sections for H + H_2 ($v = 0$, $j = 0$) → H_2 ($v' = 1$, $j' = 0-3$) + H summed over all $J \leq 10$ are plotted as a function of energy. The solid curve and solid squares do not include the geometric phase. The short dashed curve and open squares include the geometric phase and are based on the vector potential approach. The short dashed curve and open triangles are based on the calculations which ignore the geometric phase but are computed using the opposite sign for the interference terms between reactive and nonreactive contributions (see eq 24), for the para → para transitions. The data points are calculated values and the curves are a cubic spline fit.

eq 23 over the solid angle dΩ. The solid curve and solid squares do not include the geometric phase. The short dashed curve and open squares include the geometric phase and are based on the vector potential approach. For the para → ortho transitions there are no significant differences between the cross sections computed with and without the geometric phase. However, for the para → para transitions, significant differences occur between the cross sections computed with and without the geometric phase even for relatively low energies. These differences are due to the change in the sign of the interference terms between the reactive and nonreactive contributions in eq 24. This can be verified by doing the calculations *without* the geometric phase but setting $i_{gp} = 1$ in eq 24.[8] The short−long dashed curve and open triangles are based on the calculations which ignore the geometric phase but use $i_{gp} = 1$ in eq 24. We see that the short−long dashed curve and open triangles are essentially identical to the results which include the geometric phase (the short dashed curve and open squares).

Figure 11 plots the degeneracy averaged partial differential cross sections for the H + H_2 ($v = 0$, $j = 0$) → H_2 ($v' = 1$, $j' = 0-3$) + H reaction at $E_{tot} = 1.8$ eV and include all $J \leq 10$. The solid curve and solid squares do not include the geometric phase. The short dashed curve and open squares include the geometric phase and are based on the vector potential approach. For the para → ortho transitions, there are no significant differences between the differential cross sections computed with and without the geometric phase. However, for the para → para transitions, significant "out-of-phase" behavior occurs between the differential cross sections computed with and without the geometric phase. These differences are due to the change in the sign of the interference terms between the reactive and nonreactive contributions in eq 24. This can be verified by doing the calculations *without* the geometric phase but setting $i_{gp} = 1$ in eq 24.[8] The short−long dashed curve and open triangles are based on the calculations which ignore the geometric phase but use $i_{gp} = 1$ in eq 24. We see that the short−long dashed curve and open triangles are essentially identical to the results which include the geometric phase (the short dashed curve and open squares).

Figure 12 plots the degeneracy averaged partial differential cross sections for the H + H_2 ($v = 0$, $j = 0$) → H_2 ($v' = 1$, $j' = 0-1$) + H reaction as a function of total energy and include all $J \leq 10$. The results computed both with (denoted by GP) and without (denoted by NGP) the geometric phase are plotted. For the para → ortho transitions, there are no significant differences between the differential cross sections computed with and without the geometric phase for all energies. However, for the para → para transitions, significant differences occur between the differential cross sections computed with and without the geometric phase. As noted above, these differences are due to the change in the sign of the interference terms between the reactive and nonreactive contributions in eq 24 (i.e., they are due to the sign factor $(-1)^{i_{gp}}$).

Figures 10−12 show that all of the geometric phase effects cancel out in *both* the integral and differential cross sections when the contributions from even and odd values of $J \leq 10$ are added together *except* for the effects due to the sign factor $(-1)^{i_{gp}}$. The cancellation occurs for all of the energies and all of the initial and final states that we have looked at. Since the only effect of the geometric phase is the sign factor $(-1)^{i_{gp}}$, there are no geometric phase effects in the integral and differential cross sections for para → ortho or ortho → para transitions. Because the cancellation appears to be due to symmetry, we expect that these conclusions will also be valid for fully converged integral and differential cross sections. Because of the sign factor $(-1)^{i_{gp}}$, significant geometric phase effects occur for para → para or ortho → ortho transitions even for relatively low energies. These results are consistent with the predictions of Mead.[8] Mead noted that the geometric phase causes the real electronic wave function to change sign under a cyclic permutation of the three identical nuclei. This sign change gives rise to the sign change $(-1)^{i_{gp}}$ between the reactive and nonreactive contributions to the cross sections (see eqs 24 and 27).[8] Thus, the effects of the geometric phase will be significant whenever the interference between reactive and nonreactive processes is significant. The change in sign between the reactive and nonreactive contributions leads to an "out-of-phase" behavior between the results computed with and without the geometric phase. This "out-of-phase" behavior is a function of both the scattering angle and energy.

We note that our $J = 0$ results for the H + H_2 reaction based on the BKMP2 potential energy surface are in excellent agreement with those of Lepetit and Kuppermann[32] based on the LSTH potential energy surface. Our reactive and nonreactive probabilities computed both with and without the geometric phase for H + H_2 ($v = 0$, $j = 0$, $m = 0$) → H + H_2 ($v' = 1$, $j' = 0$, $m' = 0$) are nearly identical to those plotted in Figure 3 of ref 32. Also, our $J = 0$ partial integral cross sections computed

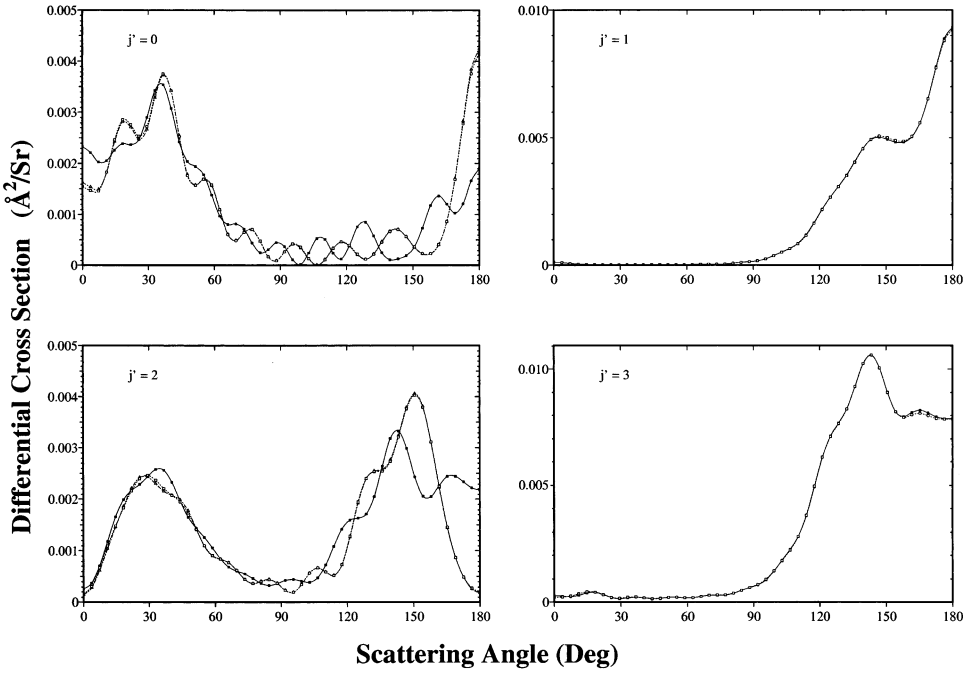

Figure 11. Degeneracy averaged partial differential cross sections for $H + H_2$ ($v = 0$, $j = 0$) → H_2 ($v' = 1$, $j' = 0-3$) + H summed over all $J \leq 10$ at $E_{tot} = 1.8$ eV. The solid curve and solid squares do not include the geometric phase. The short dashed curve and open squares include the geometric phase and are based on the vector potential approach. The short−long dashed curve and open triangles are based on the calculations which ignore the geometric phase but are computed using the opposite sign for the interference terms between reactive and nonreactive contributions (see eq 24), for the para → para transitions.

both with and without the geometric phase for $H + H_2$ ($v = 0$, $j = 0$, $m = 0$) → $H + H_2$ ($v' = 0$, $j' = 2$, $m' = 0$) and $H + H_2$ ($v = 0$, $j = 0$, $m = 0$) → $H + H_2$ ($v' = 1$, $j' = 0$, $m' = 0$) are nearly identical to those plotted in Figure 4 of ref 32. Our results and conclusions for the $H + H_2$ reaction are also consistent with those of Wu, Kuppermann, and Lepetit[33] for energies below 1.2 eV. They conclude that there are essentially no geometric phase effects in the fully converged integral and differential cross sections for para → ortho and ortho → para transitions for energies below 1.2 eV. For para → para and ortho → ortho transitions, they find "out-of-phase" behavior between the differential cross sections which are computed with and without the geometric phase. The "out-of-phase" behavior is attributed to the sign change $(-1)^{i_{gp}}$ between the reactive and nonreactive contributions to the cross sections. However, our results and conclusions for the $H + H_2$ reaction are not consistent with the results of Wu and Kuppermann[65] for energies above 1.8 eV. Wu and Kuppermann[65] predict large effects in the product rotational state distributions and integral cross sections for para → ortho and ortho → para transitions for energies above 1.8 eV. These results were initially used to help explain the discrepancies which were observed between the experiments of Kliner, Adelmann, and Zare[66] and several theoretical calculations[68−70] for the $D + H_2$ reaction (see section IV A). As noted previously at the end of section IV, the discrepancies between our results and those of Kuppermann and Wu might be related to the Eckart singularities.[51] The methodology which is used by Kuppermann and Wu is not capable of treating both Eckart singularities. An accurate treatment of *both* Eckart singularities is crucial in order to obtain accurate scattering results especially at the higher energies above 1.8 eV.[50]

V. Conclusions

We reviewed the fundamental theory for including the geometric phase in scattering and bound-state calculations based on a single adiabatic electronic potential energy surface. Two methods were discussed. In one approach, the standard Born−Oppenheimer equation for the nuclear motion is solved but with double-valued boundary conditions. In the second approach, a generalized Born−Oppenheimer equation for the nuclear motion is solved using single-valued boundary conditions. The generalized Born−Oppenheimer equation for the nuclear motion contains a vector potential which has the same mathematical properties as that of a magnetic solenoid centered at the conical intersection. Either approach is valid and will give the same results for the physical observables. In different situations, one approach may be more convenient to implement than the other.

We discussed the recently developed numerical methodology for solving the generalized Born−Oppenheimer equation for the nuclear motion. This methodology is based on symmetrized hyperspherical coordinates and can be used for both quantum reactive scattering and bound-state calculations. Several applications using this methodology were discussed. In particular, the low-energy inelastic scattering of $H + O_2$, the quantum reactive scattering of $H + D_2$, $D + H_2$, and $H + H_2$, and the vibrational spectra of HO_2 and Na_3 were discussed. The geometric phase alters the symmetry of the nuclear motion wave function causing it to simultaneously exhibit both even and odd symmetry under an interchange of any two identical nuclei. This change in symmetry gives rise to an "out-of-phase" behavior in the transition probabilities for $H + O_2$ and the reaction probabilities for $H + D_2$ and $D + H_2$. It also alters many of the lifetimes and energies of the resonances in $H + O_2$ and leads to a reordering of many of the vibrational energy levels in Na_3. Also, the symmetry change must be accounted for in order to compute the correct vibrational levels for HO_2. In the $H + D_2$ reaction, the effects of the geometric phase completely cancel out in the partial integral and differential cross sections at *all* energies when the contributions from even and odd values of $J \leq 5$ are added together. This cancellation appears to be related

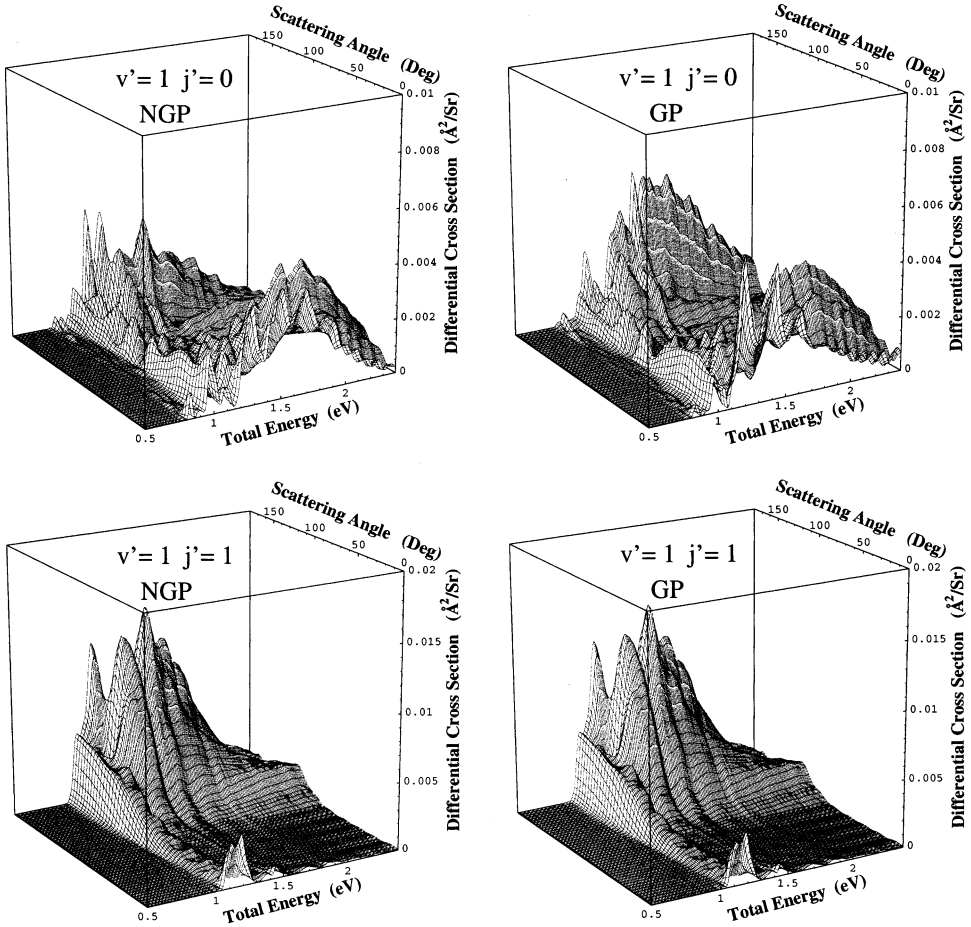

Figure 12. Degeneracy averaged partial differential cross sections for H + H_2 ($v = 0$, $j = 0$) → H_2 ($v' = 1$, $j' = 0$, 1) + H summed over all $J \leq 10$ are plotted as a function of total energy. The figures on the left do not include the geometric phase and are denoted by NGP for no geometric phase. The figures on the right include the geometric phase and are denoted by GP for geometric phase.

to the alternating symmetry of the Wigner *D* functions with respect to even and odd *J*.

We presented some new results from accurate quantum reactive scattering calculations for the D + H_2 and H + H_2 reactions. The calculations were done both with and without the geometric phase. The calculations which include the geometric phase were done using both the double-valued basis set approach and the vector potential approach. As expected, these two methods produced nearly identical results. The difference between the lowest surface function energy for DH_2 computed with and without the geometric phase alternates sign with respect to even and odd *J*. The geometric phase also gives rise to an "out-of-phase" behavior in the reaction probabilities for D + H_2. This "out-of-phase" behavior alternates "phase" with respect to even and odd *J*. The alternating sign and "phase" behavior is related to the alternating symmetry of the Wigner *D* functions with respect to even and odd *J*. The effects of the geometric phase in the D + H_2 reaction completely cancel out in the partial integral and differential cross sections at *all* energies when the contributions from even and odd values of $J \leq 19$ are added together. Recent calculations have verified that this cancellation continues to hold for all $J \leq 34$ and that there are no significant geometric phase effects in the fully converged integral and differential cross sections.[38] Significant geometric phase effects are also seen in the reaction probabilities for H + H_2 at high energies. For para → ortho and ortho → para transitions, the effects of the geometric phase completely cancel out in the partial integral and differential cross sections at *all* energies when the contributions from even and odd values of $J \leq 10$ are added together. However, for para → para and ortho → ortho transitions, significant geometric phase effects appear in the partial integral and differential cross sections summed over all $J \leq 10$ even for relatively low energies. These large geometric phase effects are due to the change in sign of the interference terms between the reactive and nonreactive contributions to the cross sections. This sign change is a direct consequence of the double-valuedness of the real adiabatic electronic wave function which changes sign under a cyclic permutation of the three identical nuclei in H_3.[8]

All of our quantum reactive scattering calculations to date for the H_3 system indicate that the effects of the geometric phase completely cancel out in both the integral and differential cross sections at *all* energies when the contributions from even and odd values of *J* are added together. Because the cancellation appears to be due to symmetry, we expect that it may also hold for other chemical reactions. Calculations for the H + O_2 → OH + O reaction are underway.[96] The only exception appears to be the para → para and ortho → ortho transitions in the H + H_2 reaction. The effects of the geometric phase at low energies for the para → para and ortho → ortho transitions were first predicted by Mead[8] in 1980. He showed that the geometric phase changes the sign of the interference terms between the reactive and nonreactive contributions to the cross sections. Thus, significant geometric phase effects can occur whenever the interference between reactive and nonreactive processes is important. Mead claimed that, for low energies, the effects of the geometric phase can be treated by doing the calculations without the geometric phase but computing the cross sections

with the opposite sign on the interference terms. However, for high energies, an accurate calculation based on the double-valued basis set approach or the vector potential approach is required. Our results indicate that Mead's procedure is probably accurate even for high energies. All other geometric phase effects in the cross sections appear to cancel out when summed over J.

We conclude that the effects of the geometric phase can be important for chemical reactions which contain three or more identical nuclei. For these reactions, the geometric phase can significantly alter the integral and differential cross sections whenever the interference between reactive and nonreactive processes is important. Furthermore, it appears that the effects of the geometric phase for these reactions can be taken into account by simply applying Mead's procedure. However, more work is needed in order to investigate the importance of the geometric phase in chemical reaction dynamics when more than one conical intersection is present (such as in the $H + O_2 \rightarrow OH + O$ reaction). More work is also needed in order to fully resolve the remaining discrepancies between the different theoretical results and experimental data for the $H + H_2$ reaction system. Because of its fundamental nature, the $H + H_2$ reaction is an excellent candidate for both theoretical and experimental studies. The differential cross sections for the para $\rightarrow$ para and ortho $\rightarrow$ ortho transitions in the $H + H_2$ reaction are probably the best candidates for an experimental confirmation of geometric phase effects in a chemical reaction.

Acknowledgment. This work was done under the auspices of the U.S. Department of Energy under Project No. 20020015ER of the Laboratory Directed Research and Development program at Los Alamos under Contract W-7405-ENG-36. Computer time on an SGI Origin 2000 at the Advanced Computing Laboratory at Los Alamos was provided by the Institutional High Performance Computing Initiative at Los Alamos.

References and Notes

(1) Born, M.; Oppenheimer, R. *Ann. Phys.* **1927**, *84*, 457.
(2) Born, M.; Huang, K. *The Dynamical Theory of Crystal Lattices*; Oxford University Press: London, 1954.
(3) Ballhausen, C. J.; Hansen, A. E. *Annu. Rev. Phys. Chem.* **1972**, *23*, 15.
(4) Mead, C. A. In *Mathematical Frontiers in Computational Chemical Physics*; Truhlar, D. G., Ed.; Springer-Verlag: New York, 1988; pp 1−17.
(5) For a recent review, see: Jasper, A. W.; Kendrick, B. K.; Mead, C. A.; Truhlar, D. G. In *Modern Trends in Chemical Reaction Dynamics*; World Scientific: Singapore, 2003.
(6) Herzberg, G.; Longuet-Higgins, H. C. *Discuss. Faraday Soc.* **1963**, *35*, 77.
(7) Mead, C. A.; Truhlar, D. G. *J. Chem. Phys.* **1979**, *70*, 2284.
(8) Mead, C. A. *J. Chem. Phys.* **1980**, *72*, 3839.
(9) Mead, C. A. *Chem. Phys.* **1980**, *49*, 23.
(10) Berry, M. V. *Proc. R. Soc. London, Ser. A* **1984**, *392*, 45. Berry, M. V. In *Geometric Phases in Physics*; Shapere, A., Wilczek, F., Eds.; World Scientific: Singapore, 1989. Berry, M. V. *Phys. Today* **1990**, *43* (12), 34.
(11) Kendrick, B.; Pack, R. T. *J. Chem. Phys.* **1996**, *104*, 7475.
(12) Bohm, A.; Kendrick, B.; Loewe, M. *Int. J. Quantum Chem.* **1992**, *41*, 53.
(13) Bohm, A.; Kendrick, B.; Loewe, M.; Boya, L. J. *J. Math. Phys.* **1992**, *33*, 977.
(14) Kendrick, B. K.; Mead, C. A.; Truhlar, D. G. *Chem. Phys.* **2002**, *277*, 31.
(15) Bishop, D. M.; Cheung, L. M. *J. Chem. Phys.* **1984**, *80*, 4341.
(16) Bishop, D. M.; Cheung, L. M. *J. Chem. Phys.* **1983**, *78*, 1396.
(17) Jensen, J. O.; Yarkony, D. R. *J. Chem. Phys.* **1988**, *89*, 3853.
(18) Chen, Y. C.; Harding, D. R.; Stwalley, W. C.; Vidal, C. R. *J. Chem. Phys.* **1986**, *85*, 2436.
(19) Mead, C. A. *Rev. Mod. Phys.* **1992**, *64*, 51.
(20) Kendrick, B.; Mead, C. A. *J. Chem. Phys.* **1995**, *102*, 4160.
(21) The global nature of the sign change can be understood topologically by realizing that within the adiabatic approximation the degeneracy manifold $\mathscr{D}$ effectively "punches a hole" in $\mathscr{M}$ so that the effective nuclear parameter space $\mathscr{M} - \mathscr{D}$ is *not* simply connected. Thus, a vector potential of the form $\mathbf{A} = (-l/2)\nabla\eta(x)$ (l odd integer) is *not* a pure gauge and therefore gives rise to a geometric phase which can lead to physical effects.
(22) The full 2π range for η is determined from the signs of the $v(x)$ and $u(x)$ functions which appear in the $\tan^{-1}$ function.
(23) Yarkony, D. R. *J. Phys. Chem.* **1996**, *100*, 18612.
(24) Yarkony, D. R. *Rev. Mod. Phys.* **1996**, *68*, 985.
(25) Yarkony, D. R. *J. Chem. Phys.* **1999**, *110*, 701.
(26) Kendrick, B.; Pack, R. T. *J. Chem. Phys.* **1996**, *104*, 7502.
(27) Simon, B. *Phys. Rev. Lett.* **1983**, *51*, 2167.
(28) Bohm, A.; Boya, L. J.; Kendrick, B. *Phys. Rev. A* **1991**, *43*, 1206.
(29) Bohm, A.; Boya, L. J.; Kendrick, B. *J. Math. Phys.* **1992**, *33*, 2528.
(30) Schutz, B. *Geometrical Methods of Mathematical Physics*; Cambridge University Press: New York, 1988.
(31) Nash, C.; Sen, S. *Topology and Geometry for Physicists*; Academic Press: San Diego, CA, 1983.
(32) Lepetit, B.; Kuppermann, A. *Chem. Phys. Lett.* **1990**, *166*, 581.
(33) Wu, Y. S. M.; Kuppermann, A.; Lepetit, B. *Chem. Phys. Lett.* **1991**, *186*, 319.
(34) Wu, X.; Wyatt, R. E.; D'Mello, M. *J. Chem. Phys.* **1994**, *101*, 2953.
(35) Kendrick, B.; Pack, R. T. *J. Chem. Phys.* **1997**, *106*, 3519.
(36) Kendrick, B. *Int. J. Quantum Chem.* **1997**, *64*, 581.
(37) Kendrick, B. K. *J. Chem. Phys.* **2000**, *112*, 5679; **2001**, *114*, 4335-(E).
(38) Kendrick, B. K. *J. Chem. Phys.* **2003**, *118*, 10502.
(39) Kendrick, B. *Phys. Rev. Lett.* **1997**, *79*, 2431.
(40) Smith, F. T. *J. Chem. Phys.* **1959**, *31*, 1352. Smith, F. T. *Phys. Rev.* **1960**, *120*, 1058.
(41) Dragt, A. J. *J. Math. Phys.* **1965**, *6*, 533.
(42) Zickendraht, W. *Ann. Phys.* **1965**, *35*, 18.
(43) Whitten, R. C.; Smith, F. T. *J. Math. Phys.* **1968**, *9*, 1103.
(44) Pack, R. T.; Parker, G. A. *J. Chem. Phys.* **1987**, *87*, 3888 and references therein.
(45) Johnson, B. R. *J. Comput. Phys.* **1973**, *13*, 445. Johnson, B. R. *J. Chem. Phys.* **1977**, *67*, 4086.
(46) Mrugała, F.; Secrest, D. *J. Chem. Phys.* **1983**, *78*, 5954.
(47) Light, J. C.; Hamilton, I. P.; Lill, J. V. *J. Chem. Phys.* **1985**, *82*, 1400.
(48) Bačić, Z.; Whitnell, R. M.; Brown, D.; Light, J. C. *Comput. Phys. Comm.* **1988**, *51*, 35.
(49) Bačić, Z.; Kress, J. D.; Parker, G. A.; Pack, R. T. *J. Chem. Phys.* **1990**, *92*, 2344 and references therein.
(50) Kendrick, B. K.; Pack, R. T.; Walker, R. B.; Hayes, E. F. *J. Chem. Phys.* **1999**, *110*, 6673.
(51) Eckart, C. *Phys. Rev.* **1934**, *46*, 383. Eckart, C. *Phys. Rev.* **1935**, *47*, 552.
(52) Kendrick, B. K. *J. Chem. Phys.* **2001**, *114*, 8796.
(53) Lehoucq, R. B.; Sorensen, D. C.; Vu, P. ARPACK: Fortran Subroutines for solving large scale eigenvalue problems, Release 2.1, available from netlib@ornl.gov in the scalapack directory.
(54) Maschoff, K. J.; Sorensen, D. C. In *Proceedings of the PARA96 Conference, Lingby, Denmark*; Wasniewski, J., Dongarra, J., Madsen, K., Olesen, D., Eds.; Springer Lecture Notes in Computer Science; Springer, New York, 1996; Vol. 1184.
(55) Lehoucq, R. B.; Sorensen, D. C.; Yang, C. *ARPACK Users' Guide*; SIAM: Philadelphia, PA, 1998.
(56) Yarkony, D. R. *J. Chem. Phys.* **1998**, *109*, 7047.
(57) Gordon, M. S.; Glezakou, V. A.; Yarkony, D. R. *J. Chem. Phys.* **1998**, *108*, 5657.
(58) Kendrick, B.; Pack, R. T. *J. Chem. Phys.* **1995**, *102*, 1994.
(59) Johnson, B. R. *J. Chem. Phys.* **1977**, *67*, 4086. Johnson, B. R. *J. Chem. Phys.* **1978**, *69*, 4678.
(60) Barclay, V. J.; Dateo, C. E.; Hamilton, I. P.; Kendrick, B.; Pack, R. T.; Schwenke, D. W. *J. Chem. Phys.* **1995**, *103*, 3864.
(61) Schön, J.; Köppel, H. *J. Chem. Phys.* **1995**, *103*, 9292.
(62) Herzberg, G. *Molecular Spectra and Molecular Structure*; Van Nostrand Reinhold: New York, 1955; Vol. I.
(63) Zhang, D. H.; Zhang, J. Z. H. *J. Chem. Phys.* **1994**, *101*, 3671.
(64) Kendrick, B. K.; Martin, R. L. (unpublished).
(65) Wu, Y. S. M.; Kuppermann, A. *Chem. Phys. Lett.* **1993**, *201*, 178.
(66) Kliner, D. A. V.; Adelman, D. E.; Zare, R. N. *J. Chem. Phys.* **1991**, *95*, 1648.
(67) Adelman, D. E.; Shafer, N. E.; Kliner, D. A. V.; Zare, R. N. *J. Chem. Phys.* **1992**, *97*, 7323.
(68) Blais, N. C.; Zhao, M.; Truhlar, D. G.; Schwenke, D. W.; Kouri, D. J. *Chem. Phys. Lett.* **1990**, *166*, 11.
(69) Mielke, S. L.; Friedman, R. S.; Truhlar, D. G.; Schwenke, D. W. *Chem. Phys. Lett.* **1992**, *188*, 359.
(70) Neuhauser, D.; Judson, R. S.; Kouri, D. J.; Adelman, D. E.; Shafer, N. E.; Kliner, D. A. V.; Zare, R. N. *Science* **1992**, *257*, 519.

(71) Kuppermann, A.; Wu, Y. S. M. *Chem. Phys. Lett.* **1993**, *205*, 577. Kuppermann, A.; Wu, Y. S. M. *Chem. Phys. Lett.* **1993**, *213*, 636E.

(72) Kitsopoulos, T. N.; Buntine, M. A.; Baldwin, D. P.; Zare, R. N.; Chandler, D. W. *Science* **1993**, *260*, 1605.

(73) Wu, Y. S. M.; Kuppermann, A. *Chem. Phys. Lett.* **1995**, *235*, 105.

(74) Kuppermann, A.; Wu, Y. S. M. *Chem. Phys. Lett.* **1995**, *241*, 229.

(75) Wrede, E.; Schnieder, L. *J. Chem. Phys.* **1997**, *107*, 786.

(76) de Miranda, M. P.; Clary, D. C.; Castillo, J. F.; Manolopoulos, D. E. *J. Chem. Phys.* **1998**, *108*, 3142.

(77) D'Mello, M. J.; Manolopoulos, D. E.; Wyatt, R. E. *J. Chem. Phys.* **1991**, *94*, 5985.

(78) D'Mello, M. J.; Manolopoulos, D. E.; Wyatt, R. E. *Science* **1994**, *263*, 102.

(79) Aoiz, F. J.; Baqares, L.; D'Mello, M. J.; Herrero, V. J.; Saez Rabanos, V.; Schnieder, L.; Wyatt, R. E. *J. Chem. Phys.* **1994**, *101*, 5781.

(80) Clary, D. C. *Science* **1998**, *279*, 1879.

(81) Seekamp-Rahn, K. *Untersuchung der Wasserstoffaustauschreaktion* $H + D_2(v = 0, j) \rightarrow HD(v', j') + D$ *in gekreuzten Molekularstrahlen*; Dissertation zur Erlangung des Doktorgrades der Fakultät für Physik der Universität Bielefeld, 1996.

(82) Schnieder, L.; Seekamp-Rahn, K.; Borkowski, J.; Wrede, E.; Welge, K. H.; Aoiz, F. J.; Bañares, L.; D'Mello, M. J.; Herrero, V. J.; Sáez Rábanos, V.; Wyatt, R. E. *Science* **1995**, *269*, 207.

(83) Siegbahn, P.; Liu, B. *J. Chem. Phys.* **1978**, *68*, 2457. Truhlar, D. G.; Horowitz, C. J. *ibid* **1978**, *68*, 2466; **1979**, *71*, 1514E.

(84) Boothroyd, A. I.; Keogh, W. J.; Martin, P. G.; Peterson, M. R. *J. Chem. Phys.* **1996**, *104*, 7139.

(85) Kuppermann, A.; Wu, Y. S. M. *Chem. Phys. Lett.* **2001**, *349*, 537.

(86) Kuppermann, A. In *Dynamics of Molecules and Chemical Reactions*; Wyatt, R. E., Zhang, J. Z. H., Eds.; Marcel Dekker: New York, 1996; pp 411−472.

(87) Wrede, E.; Schnieder, L.; Welge, K. H.; Aoiz, F. J.; Bañares, L.; Herrero, V. J. *Chem. Phys. Lett.* **1997**, *265*, 129.

(88) Wrede, E.; Schnieder, L.; Welge, K. H.; Aoiz, F. J.; Bañares, L.; Herrero, V. J.; Martínez-Haya, B.; Sáez Rábanos, V. *J. Chem. Phys.* **1997**, *106*, 7862.

(89) Wrede, E.; Schnieder, L.; Welge, K. H.; Aoiz, F. J.; Bañares, L.; Castillo, J. F.; Martínez-Haya, B.; Herrero, V. J. *J. Chem. Phys.* **1999**, *110*, 9971.

(90) Huber, K. P.; Herzberg, G. *Molecular Spectra and Molecular Structure*; Van Nostrand Reinhold: New York, 1979; Vol. 4.

(91) Zhang, J. Z. H.; Miller, W. H. *J. Chem. Phys.* **1989**, *91*, 1528.

(92) Dennison, D. M. *Rev. Mod. Phys.* **1931**, *3*, 280.

(93) Kuppermann, A.; Schatz, G. C.; Baer, M. *J. Chem. Phys.* **1976**, *65*, 4596.

(94) Schatz, G. C.; Kuppermann, A. *J. Chem. Phys.* **1976**, *65*, 4668.

(95) Miller, W. H. *J. Chem. Phys.* **1969**, *50*, 407.

(96) Kendrick, B. K. (unpublished).